NANYANG TECHNOLOGICAL UNIVERSITY SINGAPORE

Housing & Development Board

GEOBARRIER SYSTEM FOR USE IN UNDERGROUND STRUCTURE

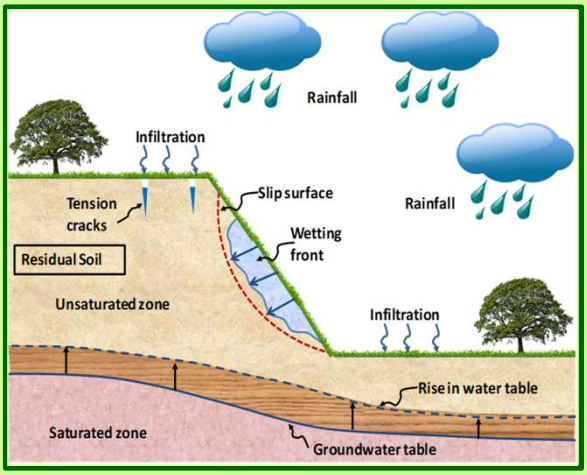

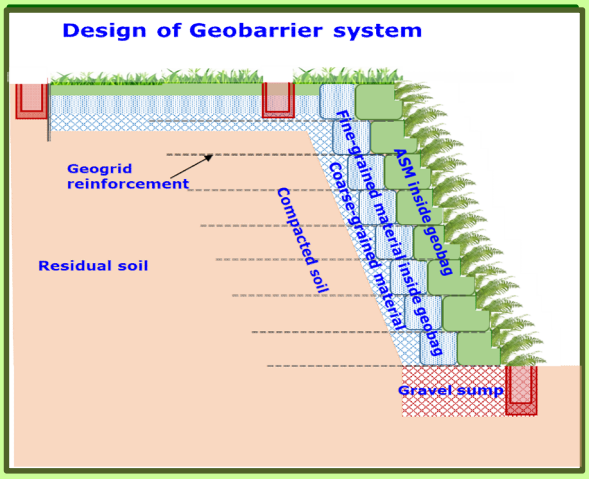

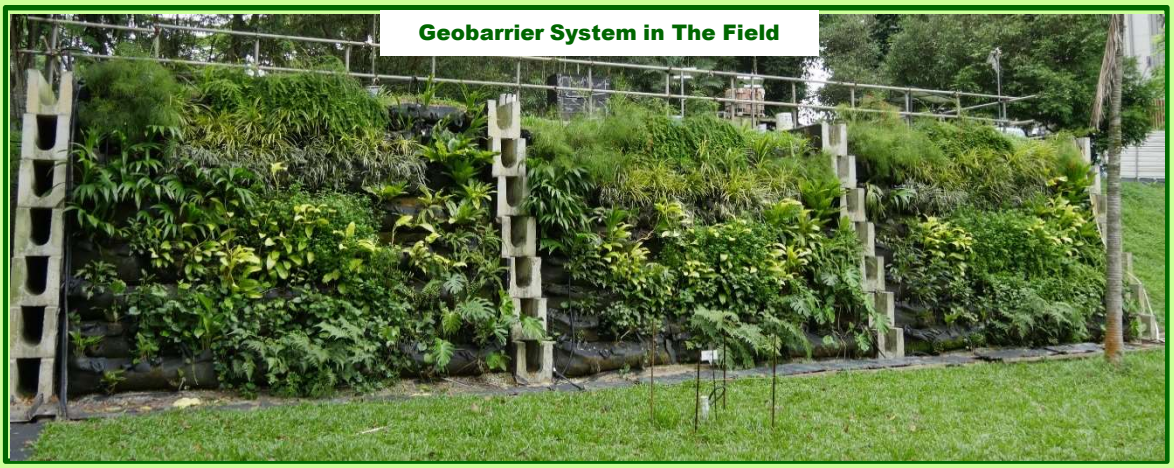

NANYANG TECHNOLOGICAL UNIVERSITY

Harianto Rahardjo
Leong Eng Choon
Alfrendo Satyanaga
Nurly Gofar
Zhai Qian
Haneena Mohamed

HOUSING DEVELOPMENT BOARD

Johnny Wong Liang Heng
Tan Sze Tiong
Wang Chien Looi
Jernice Huiling Kew
Vincent Lim Han
Seow Wei Kiong

GEOBARRIER SYSTEM FOR USE IN UNDERGROUND STRUCTURE

Research Collaboration between:

Nanyang Technological University
Housing & Development Board

Participants:

NANYANG TECHNOLOGICAL UNIVERSITY
Professor Harianto Rahardjo, Principal Investigator
Assoc. Professor Leong Eng Choon, Co-Principal Investigator
Dr. Alfrendo Satyanaga, Senior Research Fellow
Dr. Nurly Gofar, Research Fellow
Dr. Zhai Qian, Research Fellow
Ms. Haneena Mohamed, Project Officer
Dr.Yongmin Kim, Research Fellow
Er. Lim Shiyi, Research Associate
Dr. Sugeng Krisnanto, Research Fellow
Dr. Fakhrur Rozy Harnas, Research Fellow
Dr. Arun Prasad, Research Fellow

HOUSING & DEVELOPMENT BOARD (HDB)
Er. Dr. Johnny Wong Liang Heng, Group Director, Building & Research Institute
Mr. Tan Sze Tiong, Director, Environmental and Sustainability Research
Mr. Wang Chien Looi, Deputy Director, Infrastructure & Development Research
Ms. Jernice Huiling Kew, Senior Engineer, Infrastructure & Development Research
Mr. Vincent Lim Han, Senior Engineer, Infrastructure & Development Research
Mr Seow Wei Kiong, Senior Engineer, Infrastructure & Development Research

The softcopy of the monograph can be downloaded from:
www.ntu.edu.sg/library/unsaturatedsoil

The first figure (top left) on the cover shows the mechanisms of rainfall-induced slope failure. The second figure (top right) on the cover presents the schematic diagram of capillary barrier system as slope preventive measure against rainfall-induced slope failure. The third figure (bottom) on the cover shows the layout of vegetation as green cover of geobarrier system.

ISBN 978-981-11-5909-1

ACKNOWLEDGEMENT

The findings presented are based on the project "Geobarrier System for Use in Underground Structure" (Grant No. SUL2013-3) that is supported by a research grant from the Ministry of National Development Research Fund on Sustainable Urban Living, Singapore. This monograph was compiled from collaborative research projects between Nanyang Technological University (NTU) and Housing and Development Board (HDB). The monograph aims to disseminate the results and findings obtained from the research projects to the engineering community. The assistance and support provided by NTU and HDB from the initiation, the implementation until the completion of the research project are gratefully acknowledged.

The project was carried out by the School of Civil and Environmental Engineering (CEE), Nanyang Technological University (NTU) and Building Research Institute (BRI), Housing and Development Board (HDB). The excellent cooperation and coordination between NTU and HDB has resulted in the successful completion of the project. All the objectives and deliverables have been achieved within the timeframe and budget of the project. The collaborative research was carried out in such a way as to leverage the combined strengths of these two organizations.

The authors would like to acknowledge the important role played by the advisor to this project, Professor Delwyn G. Fredlund. The research has also received assistance from Tradesmen Pte Ltd., TenCate Geosynthetics Singapore Pte Ltd. SAMWOH Corporation Pte. Ltd and Eco Field Services Pte. Ltd. The contributions from NTU Geotechnical laboratory officers, Mr. Vincent Heng, Mr. Eugene Tan, and Mr. Andy Koh are greatly acknowledged.

EXECUTIVE SUMMARY

Rainfall-induced slope failures are a common problem in many tropical areas that are covered by residual soils such as Singapore. Tropical residual soils are known to be complex and their behavior does not follow the classical saturated soil mechanics because these soils are often unsaturated in nature. The negative pore-water pressure in unsaturated soil is highly influenced by the flux boundary condition changes (i.e., infiltration, evaporation and transpiration) resulting from the variation in climatic conditions. On the other hand, the negative pore-water pressure contributes additional shear strength to the unsaturated soil. As water infiltrates into the slope, pore-water pressure in the slope increases (matric suction decreases), and the additional shear strength due to matric suction will decrease or even disappear, causing the slope to be more susceptible to failure.

Singapore is a land scarce country with a critical need to optimize land utilization. Retaining walls are important part of urban development related to the creation of new spaces for urban development where land space is very limited. Conventional concrete retaining walls are usually associated with high cost, poor aesthetic and lengthy construction time. In this study, NTU collaborated with Housing and Development Board (HDB) to develop new earth retaining structure and slope stabilization system against rainfall-induced slope failures, named Geobarrier system (GBS). A GBS is a man-made three-layer cover system designed as a vegetative layer combined with a two-layer unsaturated system which harnesses the distinct difference in unsaturated hydraulic properties between a fine-grained layer and a coarse-grained layer. GBS consists of recycled materials and does not use steel nor concrete and is hence more cost effective, thereby making it economical for use in high rise building. Geobag for vegetative layer is supported by specially designed pockets for planting different types of sustainable plant species. This monograph presents the overall design, construction procedures, finite element analyses and typical results of GBS slope. In addition, apparatuses, methodology and results of the unsaturated hydraulic properties and the unsaturated shear strength are discussed briefly in this monograph.

The GBS has been designed and constructed to protect the residual soil slope from Bukit Timah Granite at Orchard. Site investigation was carried out to understand the characteristics of the in-situ residual soil prior to construction of GBS. The slope with GBS was instrumented with comprehensive field instruments (i.e. tensiometers, soil moistures sensors, pieozometer and earth pressure cell). An adjacent slope without GBS was also instrumented to investigate the performance of GBS in reducing the rainwater infiltration and maintaining the negative pore-water pressures in the slope. The numerical analyses were conducted to evaluate the readings from the instruments. The results from field instruments and numerical analyses showed that that there was no rainwater infiltration into the coarse-grained layer and soil behind GBS during rainfalls. Therefore, the GBS performed well in protecting the slope as designed. In addition, the numerical analyses results showed that the factor of safety of the slope with GBS remained relatively constant, but the factor of safety of the original slope fluctuated significantly during and after rainfall.

Table of Contents

List of Figures

List of Tables

Introduction

Background

Rapid infrastructure development in urban areas have resulted in tremendous demand for hillside developments with engineered slopes. However, slopes in tropical residual soil are prone to rainfall-induced slope failures, which can lead to damages of the infrastructures, public safety, and environmental sustainability. In addition, the cost for repairing these slopes can be quite expensive. Therefore, engineered slopes need to adopt suitable measures to prevent the failures. Combination of slope protection and retaining structure were considered in the development of Geobarrier system through collaboration research between Housing and Development Board (HDB) and Nanyang Technological University (NTU) Singapore. The appearance of Geobarrier System (GBS) was further enhanced to incorporate suitable vegetation (deep rooted grass, shrubs) as an added green cover.

Capillary barrier has been proven effective for slope protection to minimize rain water infiltration into soil slopes. A capillary barrier system is a man-made two-layer system with distinctly different hydraulic properties between a fine-grained (drainage) layer and a coarse-grained (capillary break) layer of soils. In the GBS, the capillary barrier is combined with mechanical stabilization method, utilizing geobags to encapsulate fine-grained materials and geogrids reinforcement, to augment the stability of the slope during rainfall. The system is also enhanced with proper surface drainage system and use of "green" soil cover. In line with current sustainable environment policies, recycled materials i.e. recycled concrete aggregate (RCA) and reclaimed asphalt pavement (RAP) were used as components of capillary barrier system in the GBS. Approved soil mixture (ASM) is contained in a bag and placed on top of the fine-grained layer to facilitate the planting of shrubs/trees. The performance of the GBS was evaluated under Singapore's equatorial climatic conditions through pilot field study conducted at Orchard Boulevard. Numerical analyses were carried out to model the response of the GBS to actual rainfall patterns, thus the performance of the GBS slopes could be predicted using the numerical model for different conditions related to soil properties and flux boundary conditions.

Objectives

The following objectives are outlined for this study:

1) To develop a Geobarrier system (GBS) by integrating slope protection and earth retention techniques through sustainable and environmental friendly approach.

2) To study the use of recycled environmental friendly materials i.e. recycled concrete aggregate (RCA) and reclaimed asphalt pavement (RAP) as materials within the GBS.

3) To study the use of vegetative cover on GBS to enhance the aesthetic appearance of the man-made slope.

4) To investigate the performance of the GBS through laboratory, field and numerical studies.

Methodology

The research involved five main parts, i.e., site investigation, soil and material characterization, field instrumentation, modelling and assessment of the performance of the GBS.

1) Site investigation comprises soil sampling, block sampling, and field testing (SPT).

2) A comprehensive laboratory program was conducted to evaluate basic properties, hydraulic properties, as well as saturated and unsaturated shear strength properties of in situ soil and construction materials for the GBS system.

3) Three GBS slopes were constructed and instrumented with rainfall gauge and piezometers to record rainfall and response of groundwater level to rainfall infiltration. Pore-water pressure and soil moisture measuring devices (i.e., tensiometers and soil moisture sensors) were also installed in order to study the pore-water pressure and soil moisture variations in the GBS slopes during dry and wet periods. The effects of rain water infiltration on GBS slope movements were investigated by installing load cells. Similar instrumentations were also installed in

one section of original slope in order to evaluate the performance of the GBS slopes. Data acquisition systems were used for automatic recording and supplemented by manual checks at occasional intervals.

4) Field monitoring was carried out for one year and the field performance of GBS slopes based on the field monitoring data. The performance of the three GBS slopes was compared to one section of original slope which was also instrumented with similar instrumentations and monitored for one year.

5) Deformation-seepage modelling was performed using a saturated-unsaturated finite element program. The model provided insight to the pore-water pressure distributions in GBS slopes as compared to the original slope under the flux boundary conditions measured during the field monitoring periods. The results of the seepage modelling was compared to the pore water pressure and volumetric water content data collected during the monitoring period. The results of the deformation analysis was compared to the earth pressure measurements by earth pressure cells. The deformation analysis has accounted for the effect of changing pore-water pressure on the deformation pattern of the GBS as an earth retention system.

6) The stability of the GBS slopes was investigated by incorporating the results from the seepage modelling. The analyses provided information on the change in the factor of safety of the GBS slopes and original slopes with time under various rainfall conditions and properties of soil behind GBS. Tensile stress developed in the reinforcement of GBS slopes was deduced from the output of the stability analysis and was compared to the results of field test.

Design of Geobarrier System

Theoretical Concept of Geobarrier System

Reinforced soil walls have been used to stabilize near vertical slopes because the method requires less cutting and filling, reduces construction time and is usually more cost effective. This method offers mechanical stabilization of the near vertical slopes, but the

performance of this type of wall depends primarily on the quality of fill material, drainage system and construction procedures (Koerner, 2012). The reinforced soil walls comprise three components i.e. reinforced fill, reinforcing elements, and wall facing. Geobags wall is one type of reinforced soil wall which utilizes stacked bags of soil as facing panels and reinforcing elements to hold the weight of soil behind it (Ansari et al., 2001; Matsuoka and Liu, 2006; Yoo and Jung, 2006). The performance of reinforced soil walls depends primarily on the quality of fill material, drainage system and construction procedures (Koerner and Koerner, 2013). Failures of reinforced soil wall triggered by rainfall infiltration have been reported by Yoo and Jung, 2006; Liu et al, 2012; Koerner and Koerner, 2013. Thus the challenge in geobag type of wall is the improper drainage system and the quality of fill material used within the geobags.

Capillary barrier is an effective method to minimize rain water infiltration into soil slopes; thereby maintaining the suction within the reinforced soil. (Rahardjo et al., 2012). The capillary barrier is a man-made two-layer cover system comprising a fine-grained (drainage) layer and a coarse-grained (capillary break) layer of soils. Geobarrier system (GBS) was developed by Rahardjo et al. (2015) to combine the mechanical stabilization offered by the reinforced soil wall and the protection from rainfall infiltration offered by the capillary barrier system. Research on the capillary barrier as a slope protection system has been in progress since 2002 and the results can be found in various publications i.e. Tami et al. (2002; 2003; 2004a,b); Yang et al. (2004); Krisdani et al. (2005; 2006; 2010); Indrawan et al. (2010); Harnas et al. (2014a,b; 2016a,b); Rahardjo (2015); Rahardjo et al. (2006; 2007a; 2010; 2012a,b; 2013b,c, 2016; 2018b).

The GBS comprises three layers: top layer consists of approved soil mix (ASM); middle layer consists of fine-grained materials; and bottom layer consists of coarse-grained material. The ASM is contained in geobags and placed on top of the capillary barrier system to facilitate the planting of vegetation. For the near vertical slope, the fine-grained material is also encapsulated with the geobags and connected to geogrids reinforcement, to augment the stability of the slope. The coarse material is laid in between the reinforced soil fill and the geobags of fine-grained materials. Rahardjo et al (2018b) showed that the presence of geobags between the fine- and coarse-grained material did not interfere the effectiveness

of the capillary barrier system. Both bags of ASM and fine materials are connected to high tensile strength geogrids in order to retain the wall through the friction between the geogrids itself and the reinforced fill behind the capillary barrier system.

Previous studies by Rahardjo et al. (2013) and McCulloch et al. (2017) showed that recycled materials can be used to replace natural materials forming the capillary barrier system. Therefore, in line with current sustainable environment policies, recycled materials were used as components of capillary barrier system in the GBS. Approved soil mixture (ASM) was also contained in geobag and placed in front of the fine-grained layer to facilitate the planting of deep and widespread rooted shrubs/trees. The reinforced fill is made of compacted residual soil. The system was also enhanced with proper drainage system through gravel sump below the toe of the slope. The sump is located at the bottom of the GBS slope to collect the rainwater from fine-grained layer and drain it out to main drainage. The cross-sectional view of GBS is shown in Figure 1.

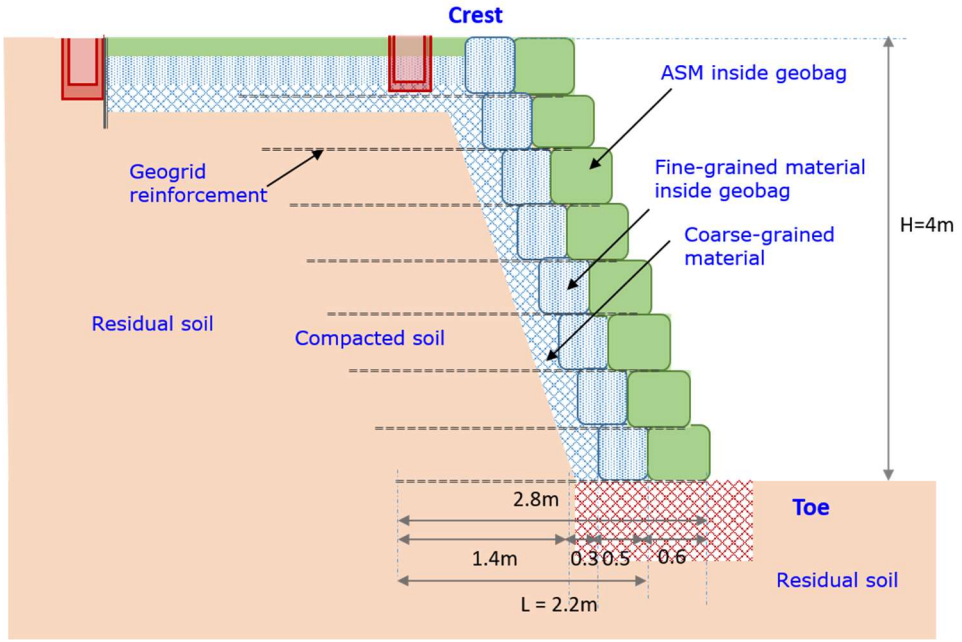

Figure 1: Schematic diagram of Geobarrier system (GBS)

Selection of Materials for Geobarrier System

Recycled concrete aggregates (RCA) and reclaimed asphalt pavement (RAP) were used for the construction of GBS. The fine-grained material (fine RCA or fine RAP) was wrapped in a geobag and stacked on top of each other on the wall face to form a retaining wall. Coarse RCA or coarse RAP was placed behind the geobags to limit water infiltration into the compacted residual soil. The materials used for the construction of the GBS were selected in such a way that the system will not cause any adverse effect to the environment. Toxicity characteristic leaching procedure (TCLP) were conducted on the RCA and RAP to ensure that the discharge from GBS will not cause contamination. The test results showed that both RCA and RAP used in the Pilot study did not contain any hazardous chemical. The RCA and RAP used for the construction of GBS at the pilot study site are shown in Figure 2.

Figure 2. RCA and RAP used for construction of GBS at Pilot study site

The suitability of ASM as planting material was evaluated based on pH, electrical conductivity as well as soil texture. The ASM is the mixture of topsoil, sand, soil conditioner and organic compost. The topsoil is a free draining soil of a workable crumbly lump free loamy character and contains no grass or weed growth of any kind or other foreign material or stones exceeding 25 mm in diameter. The topsoil should be reasonably free from calcium carbonate, subsoil, refuse, roots, clods, phytotoxic materials and other deleterious substances. It is also fertile, friable soil, nontoxic and capable of sustaining healthy plant growth. The sand used in ASM should be free of any debris, stones or other foreign material. The soil conditioner is Peat Moss, organic compost or other fibrous organic matter suitable for mixing with topsoil to make a friable growing medium for plants, resistant to rapid decay and free of large lumps or debris. Organic composts are derived from organic vegetable parts of plants (preferably leaves), and produced by a thorough horticultural or industrial composting process. Texture of compost to be used in ASM is fine and friable, free from any rotting substances, debris, refuse, clay or visible fungus/ pathogens/pests without any intense obnoxious odors. The ASM to be used in used in GBS should follow the criteria outlined in Table 1.

Table 1: Proportion and specification of Approved soil mix (ASM) (NParks, 2013)

No.	Parameters	Required Range/Value
1.	Soil components by volume	
	Topsoil	50%
	Sand	20%
	Soil conditioner	15%
	Organic compost	15%
2.	pH	5.5 to 7.8
3.	Electrical Conductivity	Not exceeding 1500 micromho/cm (1500 microSiemens/cm)
4.	Soil-water extract	1:2.5 (w/v)
5.	Topsoil Texture/components	
	i) Sand	Particle size: between 0.05 to 2mm. Proportion: from 20% to 75%.
	ii) Silt	Particle size: between 0.002 to 0.05mm. Proportion: from 5% to 60%.
	iii) Clay	Particle size: less than 0.002mm. Proportion: from 5% to 30%.

The configuration of the capillary barrier should be evaluated based on criteria proposed by previous researchers. Smersud and Selker (2001) suggested a criterion based

on coefficient of uniformity and ratio of particle size (defined as d_{50} i.e. the diameter of the particle where 50% by weight of the particles have smaller diameter) of the coarse- and fine-grained material. Furthermore, Rahardjo et al. (2007, 2013) suggested three factors to be considered in the design of the CBS: i) the water-entry value, ψ_w, of the coarse-grained soil (preferably <1 kPa); ii) the ratio between the water-entry value of the fine-grained layers and the coarse-grained layers (ψ_w-ratio) preferably to be greater than 10, iii) the saturated coefficient of permeability of the fine-grained non-cohesive soil (preferably $>10^{-5}$ m/s).

GBS uses in-situ soil as reinforced soil. The soil should be compacted to 90% dry density based on laboratory compaction curve. The actual compaction level should be checked in-situ for each placement layer of soil using sand cone test (ASTM D7830/D7830M-14).

Geotextile used in manufacturing the geobags consisted of a woven monofilament fiber weaved to form a stable matrix with high water flow and optimum opening size for soil retention. The specifications of geotextile bag for GBS are as follows: (i) Tensile strength of the geotextile should be greater than or equal to 50 kN/m; (ii) California Bearing Ratio (CBR) puncture strength of greater than or equal to 5.0 kN; (iii) Pore size (O_{90}) of less than or equal to 600 microns; (iv) Water permeability greater than or equal to 200 L/m^2/s (0.2 m^3/s per m^2).

The dimension of geobag for ASM is 0.6 m width × 0.5 m height × 1.5 m length while the dimension of geobag for fine grained material is 0.6 m width × 0.5 m height × 0.75 m length. The presence of geobag at the interface between the fine- and coarse-grained material should not interfere with the effectiveness of the capillary barrier system. Both bags are connected to 2.8 m anchorage tail. Figure 3 shows the geobags used for ASM and fine-grained material which are connected to geogrids. The bi-axial geogrids used as reinforcing element should be made from high quality polyester yarn fibers with high tensile strength with a design life of 120 years and a tensile strength of 12 kN/m @ 2% strain and 30 kN/m @ 5% strain. The geobags for ASM were supplied with planting sleeves and stitches for designated planting holes (Figure 4). Provisions for plantings were provided such that cuts could be made to create openings to allow planting that will form

the vegetative cover for the GBS. The sizes of the openings were designed to be just large enough to accommodate the root balls of the plants.

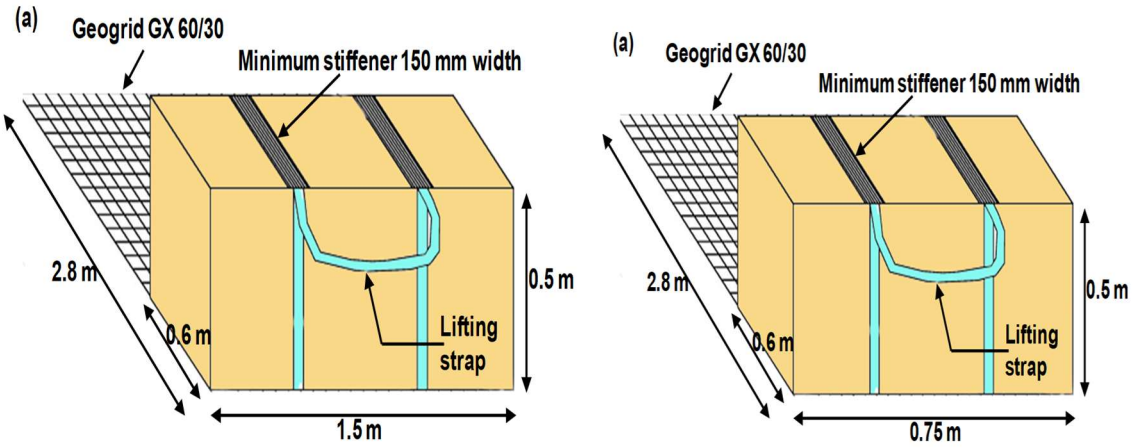

Figure 3: Geotextile bags for (a) ASM and (b) fine grained material

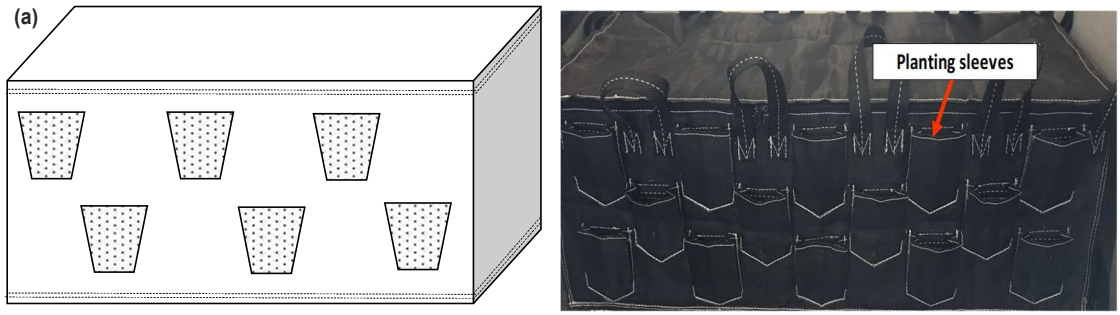

Figure 4: Planting sleeves in front of ASM bags

Specification of Plants

The plants to be used as green cover in GBS are classified as deep rooted grass and small shrub. Deep-rooted grass need minimal irrigation, fertilizer or maintenance. Some of them grow quickly from seed while others are laid more successfully as sod. When deep-rooted grass grows well, they can reach 150–400 mm high and 150–400 mm diameter. The number of plants per 1 square meter is 14–5. There are many varieties of deep-rooted grass and small shrub, however the species of plants are suggested for the green cover of the GBS are shown in Table 2. The appearance of a completed GBS system with green cover is shown in Figure 5.

Figure 5: Appearance of GBS with green cover

Table 2: Species of plants for green cover of GBS

No	Type/Name	Height (mm)	Spread (mm)	No/m^2
1	Russelia equisetiformis	350	350	5
2	Xiphidium caeruleum	300	340	5
3	Epipremnum aureum	150	200	14
4	Calathea loeseneri	275	290	5
5	Phyllanthus cochinchinensis	200	250	14
6	Wedelia trilobata	180	160	14
7	Philodendron erubescence	200	200	14
8	Piper sarmentosa	200	150	14
9	Hymenocallis speciose	350	300	5
10	Ophiopogon jaburan ‘Variegata’	160	170	14
11	Nephrolepis exaltata	300	320	5
12	Davallia denticulate	300	250	14
13	Pandanus pygmaeus	180	250	14
14	Asplenium nidus	300	350	5
15	Philodendron Xanadu	250	350	5
16	Monstera Deliciosa	400	400	5

Site Investigation

Pilot study of GBS in the field was carried out at a state land in the southern part of Singapore island. The slope is located at an area surrounded by Orchard Boulevard, Orchard Spring Lane, Cuscaden Road on three sides and by private residential properties on the fourth side. Figure 6 illustrates the location of the pilot study at Orchard Boulevard, Singapore. Site investigation program for the construction of GBS in this pilot study include (1) Topographical survey, (2) Identification of general soil condition, (3) Soil sampling (4) Laboratory tests.

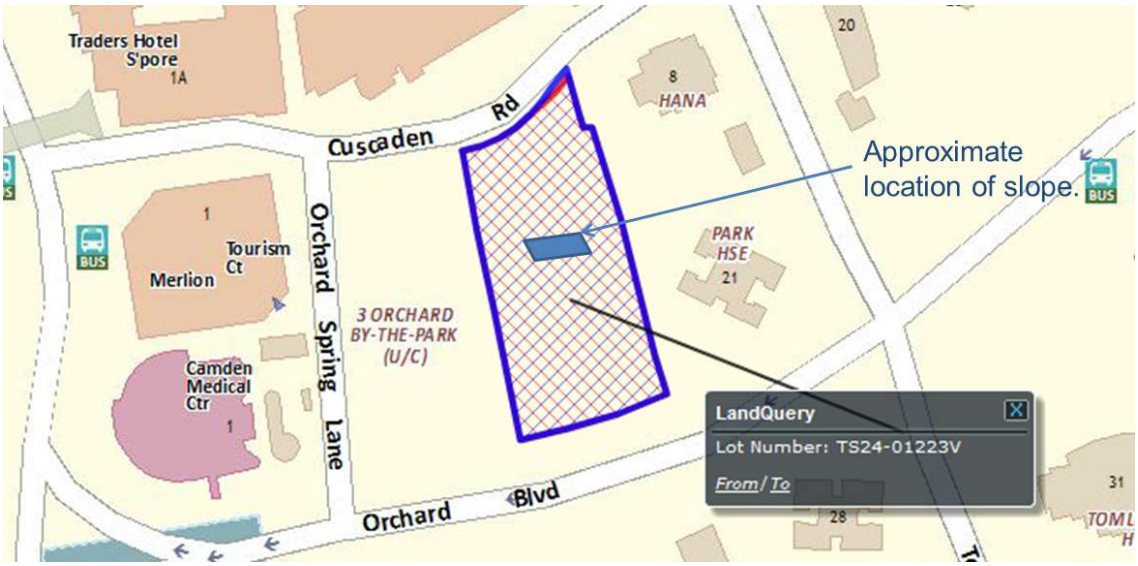

Figure 6: Location of Pilot study of Geobarrier system

Topography and General soil condition

Topographical surveys were performed to establish the relief of the sites for the construction of the GBS. The original soil slope from Bukit Timah Granite poised at a slope angle of approximately 35° with an average elevation difference of 4m. Figure 7 show the original topography of the pilot study at Orchard Boulevard.

Six numbers of boreholes (BH1 - BH6) were drilled at Orchard Boulevard site as shown in Figure 7 to observe the geology, soil stratification and in-situ properties of

the soil. The boreholes were advanced using rotary boring. Standard penetration tests (SPT) were conducted in the borehole at an interval of 1 m. The borehole was terminated if rock was encountered or the SPT 'N' value was greater than or equal to 100.

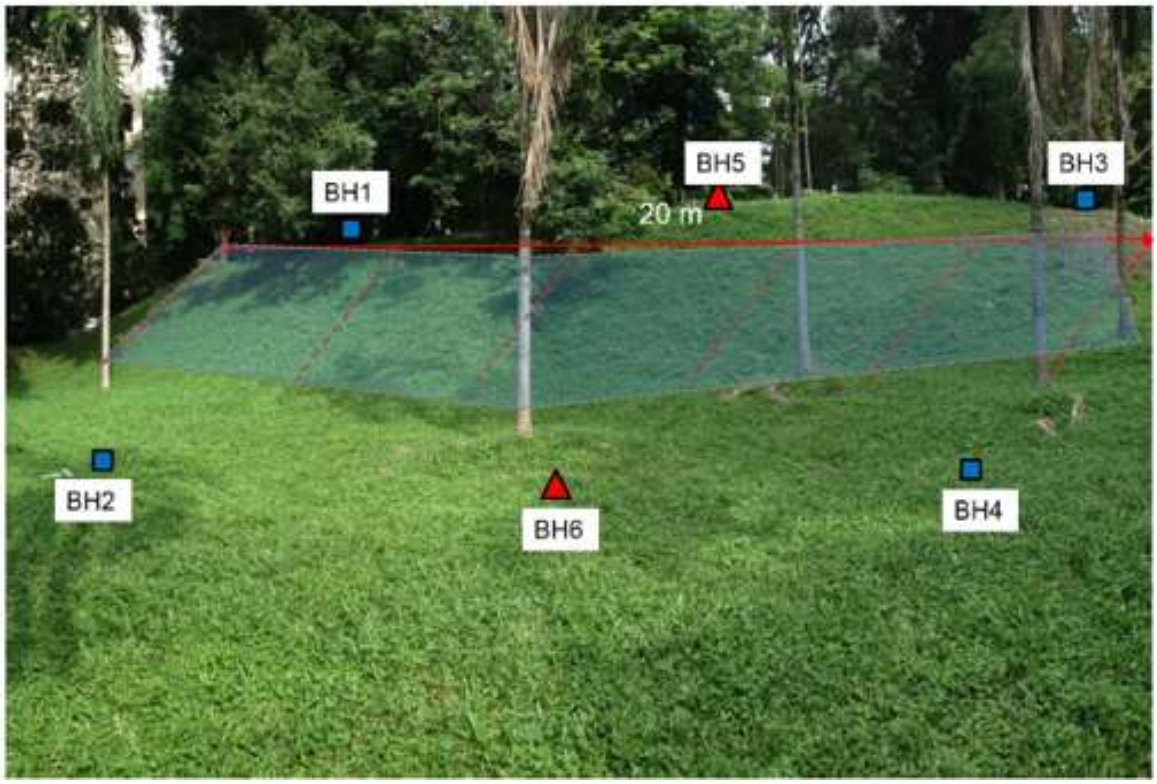

Figure 7: Original slope condition and borehole locations at Pilot study site

Bore-logs were prepared for the identification of the geology and the soil stratification at the site. Based on the soil stratification derived from the six bore-logs, the soil at Orchard Boulevard can be divided into three different layers of residual soil, named Layer 1, Layer 2 and Layer 3. The SPT-N values increased with depth from 4–5 in Layer 1 to 11–19 in Layer 3. Based on the Unified Soil Classification System (USCS) as described in ASTM D2487-00, soils in Layer 1 and 2 are classified as CH (clays with high plasticity) while the soil in layer 3 is classified as CL (clay with low plasticity). The bedrock comprising Bukit Timah Granite was obtained at depth of 10 m below ground surface. Simplified soil profiles representing the soil stratification at Orchard Boulevard

site is presented in Figure 8. Groundwater table was estimated at depth of 3m below the ground surface at crest and 2 m below ground surface at toe.

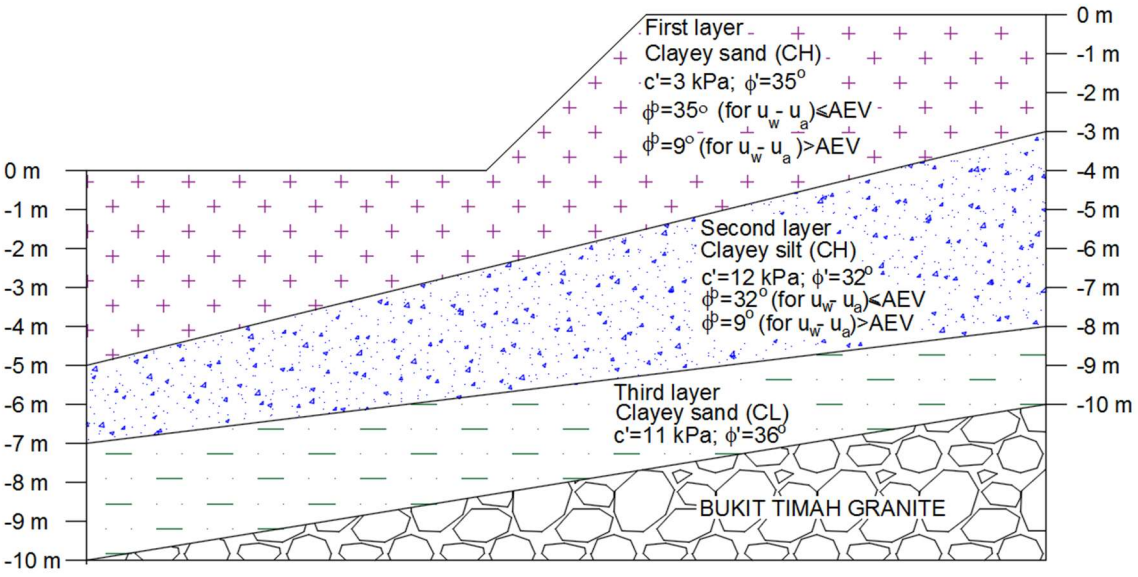

Figure 8: Simplified soil profile of residual soil slope at Pilot study site

Soil Sampling

Undisturbed samples were obtained using 75 mm diameter thin walled sampler at interval of 1 m from the borehole. In order to minimize disturbance, the samples were obtained by hydraulically pushing the tube to the required depth, however; if hard soils were encountered, the samples were collected by driving the open drive sampler with hammer. Disturbed samples were taken from the split spoon sampler (from SPT test) for soil description and classification. In addition, block samples (300mm×300mm×300 mm) were also retrieved in order to obtain representative samples near ground surface. The block samples were wrapped using a cling-film and encased in wooden box while the sample was still attached to the ground.

Soil and Material Characterization

Laboratory tests were performed on undisturbed samples obtained from the pilot study site as well as materials used for the construction of GBS slopes, i.e. compacted residual soil, fine and coarse RCA, fine and coarse RAP, ASM and Gravel. The laboratory tests comprised of index properties tests, grain-size distribution, compaction test, soil-water characteristic curves (SWCC), saturated and unsaturated permeability, as well as saturated and unsaturated triaxial tests.

Index Properties and Grain-size distribution

The index properties tests that were carried out according to ASTM D4318–00 on residual soil as well as materials used for the construction of GBS slopes. The index properties required for the construction and analysis of the GBS are (i) Natural water content; specific gravity (G_s); Atterberg limits (LL, PL and PI), and grain-size distribution. The soil samples were classified under the Unified Soil Classification System (USCS) using the information from the index properties tests. The specific gravity of the residual soil is similar for all layers i.e. 2.67, while the dry density is between 1.35 and 1.39 Mg/m^3. The natural water content increases from 0.32 in Layer 1 to 0.33 in Layer 2 and 0.36 in Layer 3. Thus the total density of the residual soil is between 1.80 – 1.85 Mg/m^3. Since the properties of all layers are almost similar and the Layer 1 is quite thick, only the properties of Layer 1 will be discussed further. The index properties of residual soil obtained at the pilot study site and the construction materials are presented in Table 3. The coefficients of saturated permeability of residual soil and the materials used for the construction of GBS are also presented in Table 3.

Grain-size distribution curves were obtained from the combination of mechanical sieve analyses and hydrometer tests (for fine particle or particle size < 75 um). The wet sieving analyses were performed to determine the fine content. Typical grain-size distribution curves were calculated based on the average percentage passing of each particle diameter. Based on the grain-size distributions, the residual soil in Layer 1 can be classified based on USCS (ASTM D2487-00) as highly plastic clayey sand (CH) while coarse RCA and coarse RAP can be classified as poorly graded gravel (GP) while fine

RCA and fine RAP can be classified as poorly graded sand (SP). The ASM can be classified as clayey sand (SC) while gravel used for the construction of sump can be classified as poorly graded gravel (GP). The grain-size distributions of the residual soil as well as the construction materials for GBS slopes are plotted in Figure 9.

Table 3: Index Properties of residual soil and construction materials of GBS slopes

Description	Residual soil	ASM	Fine RCA	Coarse RCA	Fine RAP	Coarse RAP	Gravel
USCS**	CH	SC	SP	GP	SP	GP	GP
Specific gravity, G_s	2.67	2.41	2.57	2.66	2.40	2.53	2.69
Gravel content (%)	32	0			0	100	100
Sand (%)	5	76	0	100	100	0	0
Silt (%)	47	8	100	0	0	0	0
Clay (%)	17	16	0	0	0	0	0
Liquid Limit, LL (%)	31	16	NA*)	NA	NA	NA	NA
Plastic Limit, PL (%)	52	41	NA	NA	NA	NA	NA
Plasticity Index, PI (%)	21	25	NA	NA	NA	NA	NA
Dry density, ρ_d (Mg/m^3)	1.37	1.18	1.67	1.57	1.62	1.53	1.65
Saturated coefficient of permeability, k_s (m/s)	1×10^{-7}	1×10^{-5}	1×10^{-3}	4×10^{-3}	4×10^{-4}	1.2×10^{-3}	5×10^{-1}

*NA= not applicable **) Unified Soil Classification System (USCS) is described in ASTM D2487 (2000)

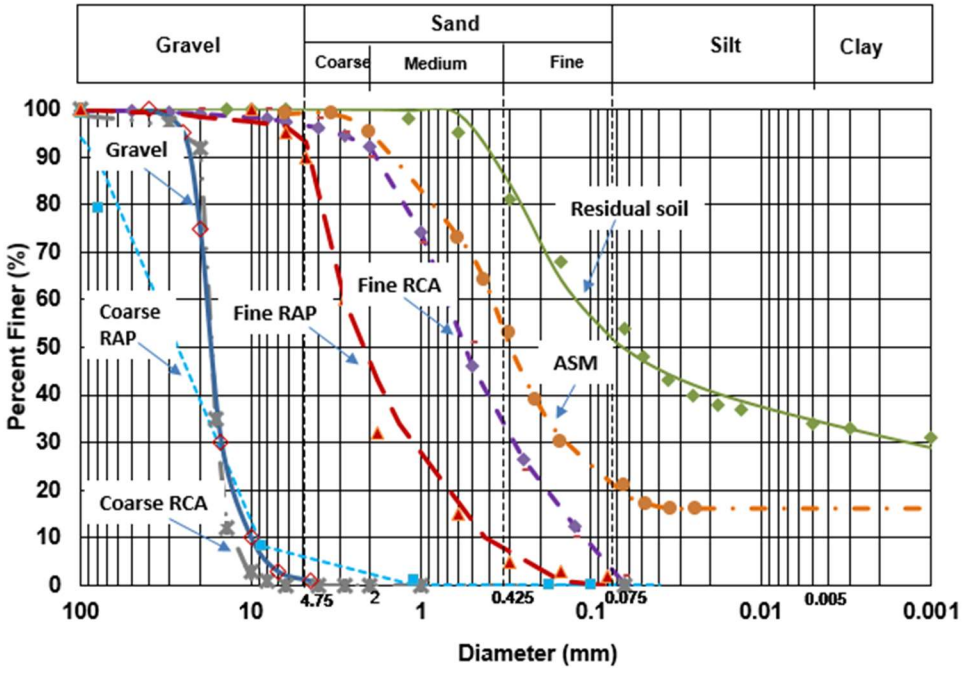

Figure 9: Grain size distribution of residual soil and GBS construction material

The reinforced soil was derived from in-situ residual soil. The soil was compacted to 90% of compaction level based on the maximum density obtained from laboratory compaction curve. The compaction test was carried out following ASTM D698-12. Figure 10 shows the compaction curve of residual soil from Layer 1. Based on the compaction curve, the maximum dry density and optimum water content for the compaction of the residual soil are 1.92 Mg/m^3 and 10%, respectively. For the pilot study, the soil was compacted at dry density of higher than 1.73 Mg/m^3 and water content of 15.1%.

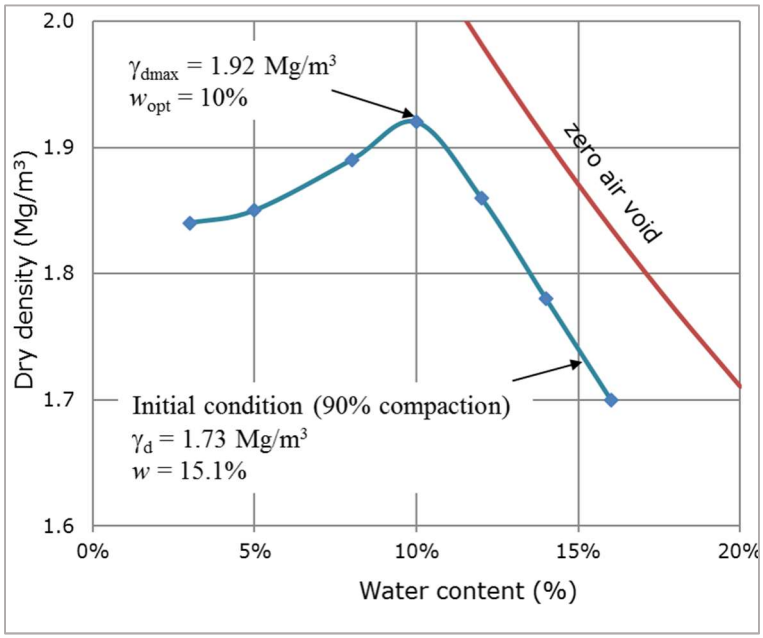

Figure 10: Laboratory compaction curve for reinforced soil fill

Soil-water characteristic curves

Soil-water characteristic curves (SWCC) is an important soil property in unsaturated soil mechanics. It relates water content to the matric suction (u_a-u_w) of the soil. The SWCC was conventionally measured using Tempe cell, pressure plate and salt solution methods. However, these tests are tedious and time consuming (Agus et al., 2001; Xiaoli et al., 2011; Fredlund et al., 2012; Leong and Wijaya, 2015). Some recently developed apparatuses such as Hyprop, small-scale centrifuge and dew-point chilled mirror were used in this study to determine the SWCC. The schematic diagrams for each apparatus are shown in Figures 11 to 16. Each technique can be used for different range of suction as shown in

Figure 17. The details and procedures of SWCC tests using Hyprop is explained in Schiendler et al (2010) while the other methods are standardized in ASTM D6838-02.

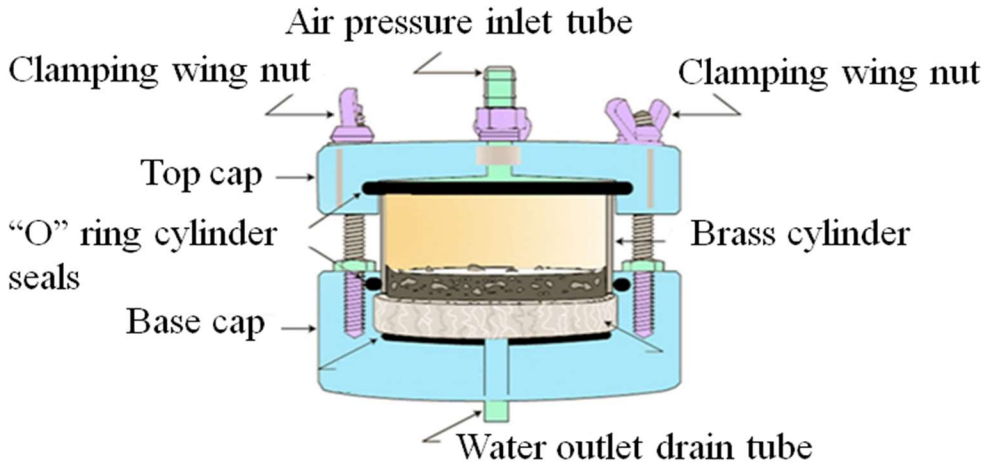

Figure 11: Schematic diagram of Tempe cell (Rahardjo et al, 2007b)

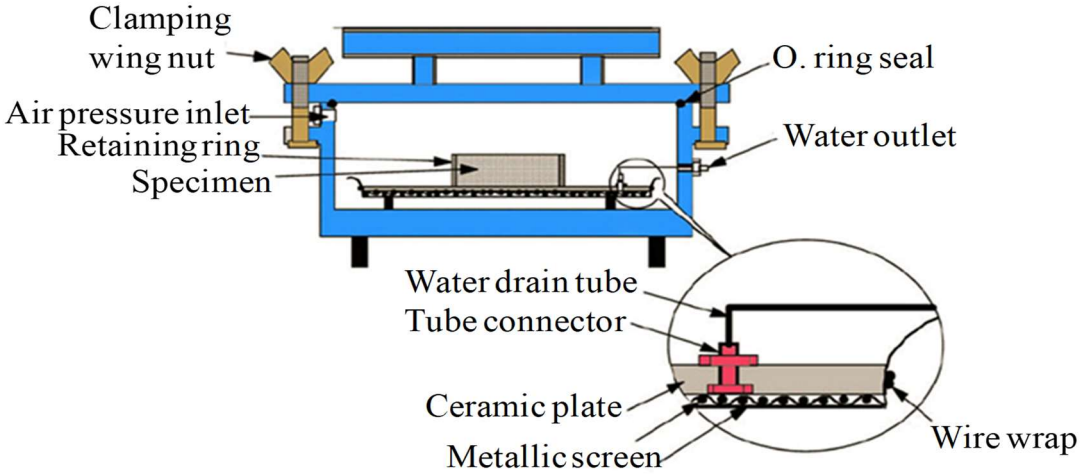

Figure 12: Schematic diagram of pressure plate (Rahardjo et al, 2007b)

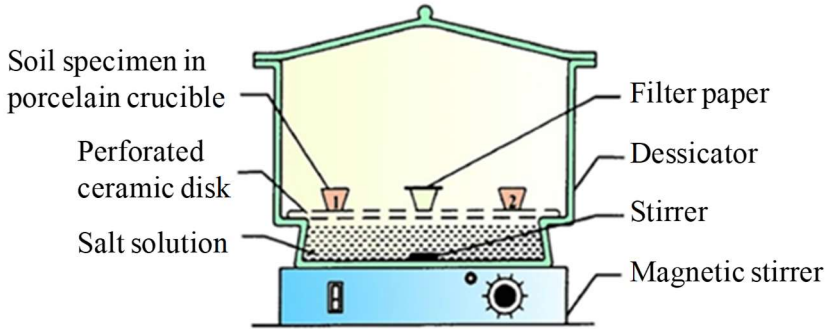

Figure 13: Schematic diagram of salt solution test apparatus (Agus et al, 2001)

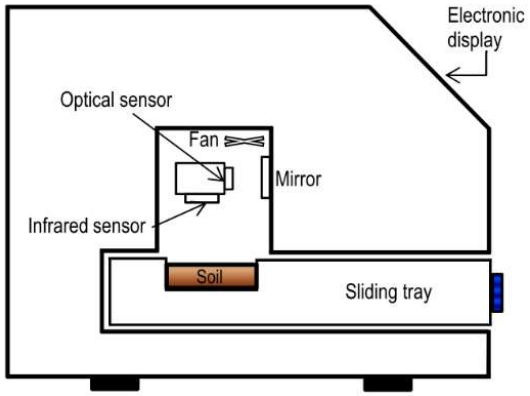

Figure 14: Schematic diagram of dew point method apparatus

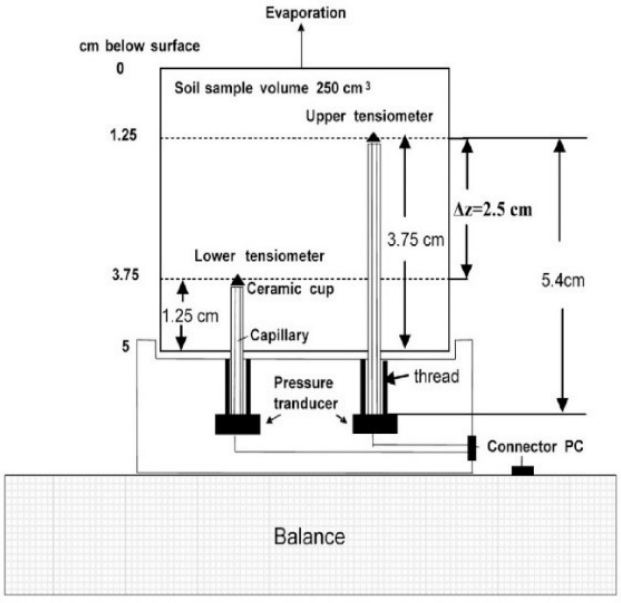

Figure 15: Schematic diagram of hyprop apparatus (Schindler et al, 2010)

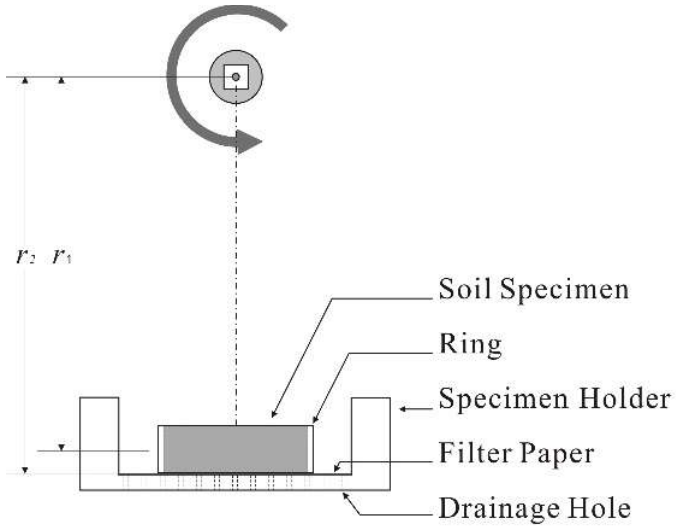

Figure 16: Schematic diagram of mini centrifuge apparatus (Rahardjo et al, 2018a)

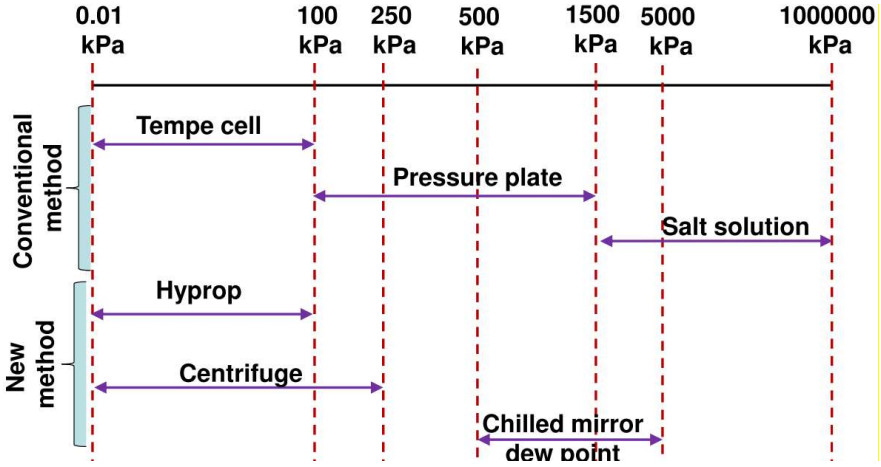

Figure 17: Range of suction applicable for SWCC measurement techniques

Most apparatuses can be used to perform SWCC test for drying process. However, it is important to plot the SWCC for drying and wetting process because most of the geotechnical problems, such as slope failure, are induced by rainfall that generally causes a wetting process in soil. Thus, the SWCC tests were carried out in this study under both drying and wetting processes using various apparatuses available at NTU Geotechnics Laboratory. The SWC drying curves of residual soil from the pilot study site as well as construction materials for GBS slopes are presented in Figure 18 while the wetting curves

are presented in Figure 19. The fitting parameters and SWCC parameters of residual soil and all materials involved in the construction of the GBS at Orchard Boulevard are summarized in Table 4.

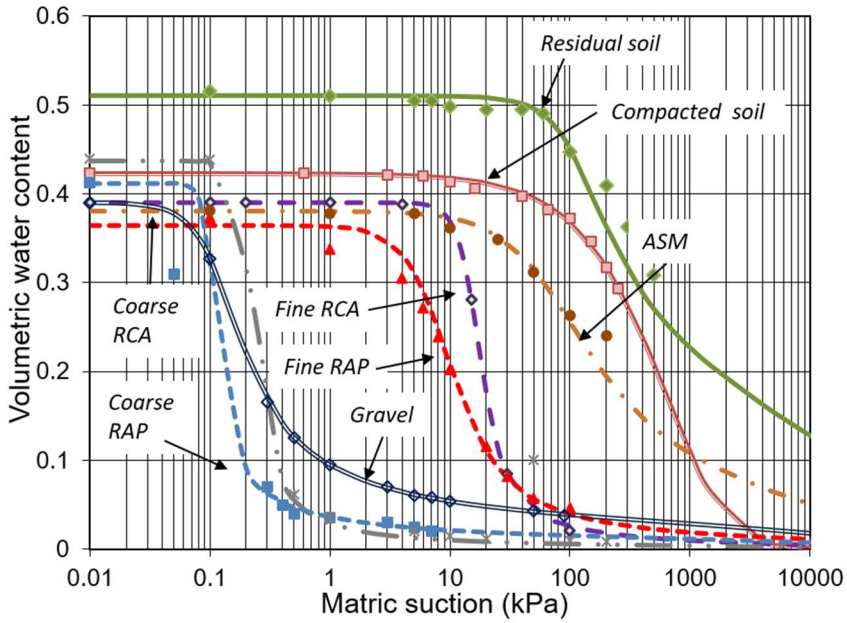

Figure 18: Drying SWCC of in-situ soil and construction materials of GBS slopes

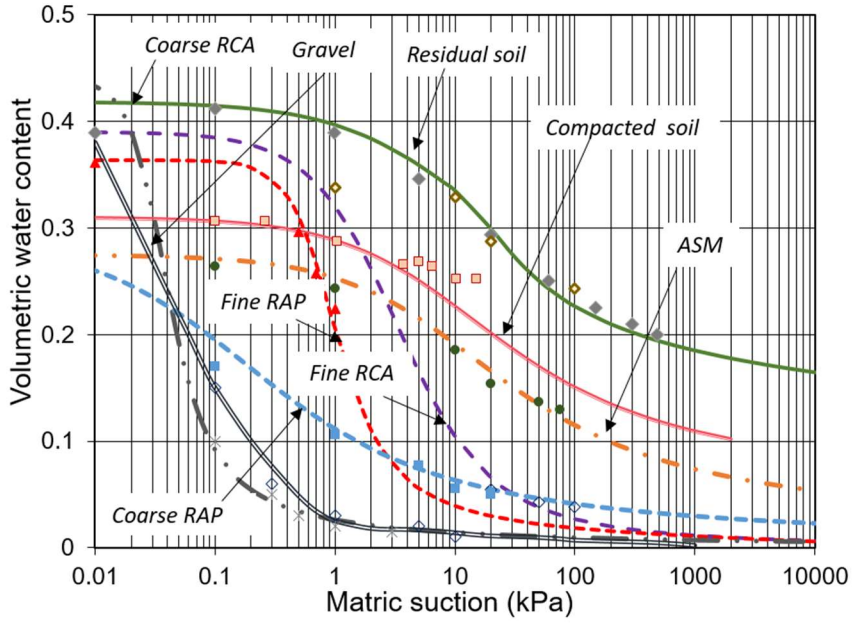

Figure 19: Wetting SWCC of in-situ soil and construction materials of GBS slopes

Table 4: SWCC parameters of in-situ soil and GBS construction materials

Fitting Parameters	Residual soil	ASM	Fine RCA	Coarse RCA	Fine RAP	Coarse RAP	Compacted residual soil	Gravel
a(kPa)	24.9	56.11	10	0.171	7.17	0.098	1630	0.11
n	0.73	1.55	5	4.56	2.439	9.619	1.06	2.72
m	0.41	0.785	2	0.933	1.192	0.784	7	0.79
Sat. Vol. Water content θ_s	0.51	0.381	0.39	0.437	0.364	0.412	0.423	0.39
Air entry value (kPa) ψ_a	64	25.65	7.02	0.129	4.0	0.085	112.5	0.064
Residual suction (kPa) ψ_r	632	418.3	16.24	0.429	2.94	0.171	1576	0.568
Vol Water content at Residual suction θ_r	0.21	0.124	0.429	0.031	0.024	0.027	0.042	0.065
Water entry value (kPa) ψ_w	60	1000	30	0.6	1000	0.2	100	1

Permeability function

The determination of unsaturated coefficient of permeability by experiment is a tedious and time-consuming process. Therefore, an indirect method using a statistical model is commonly used to predict the permeability function from the saturated coefficient of permeability, k_s, and the soil-water characteristic curve (Fredlund and Xing, 1994; Marshall, 1958; Millington and Quirk, 1959, 1961; Kunze, 1968; Green and Corey, 1971). The calculated permeability data can then be fitted using the mathematical equation as suggested by Leong and Rahardjo (1997). In this study, the drying and wetting permeability functions were both considered. However, previous study (Tami et al, 2004) showed that wetting permeability function is more suitable for the study of rainfall infiltration under both drying and wetting conditions. Figures 20 shows the wetting permeability functions of the residual soil and all construction materials used for the construction of GBS at the pilot study site.

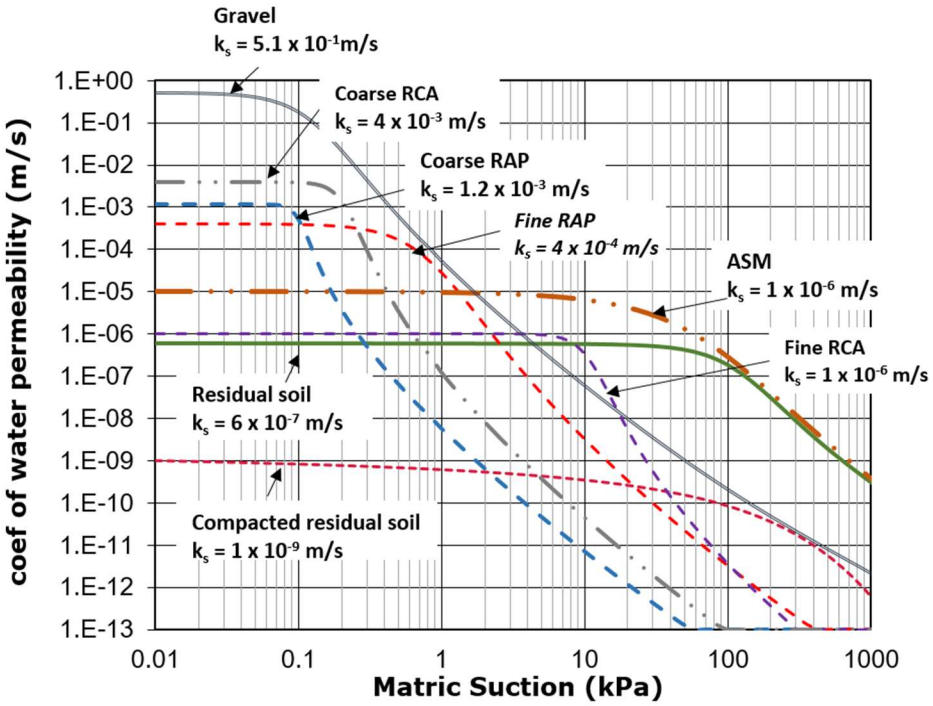

Figure 20: Permeability functions of residual soil and GBS construction materials

Saturated and unsaturated shear strength

Saturated shear strength parameters (c' and ϕ') were obtained from consolidated isotropically undrained (CU) saturated triaxial testing with pore-water pressure measurement. The multi-staged saturated triaxial tests were performed in accordance with ASTM D4767-11 to obtain the saturated shear strength of residual soil and other construction materials used for GBS. Two failure criteria were selected according to Head (1986): (1) Maximum deviator stress, and (2) Maximum principal stress ratio (σ_1'/σ_3') had been reached. The shear strength parameters of residual soil and the materials used for the construction of GBS are presented in Table 5.

Unsaturated shear strength parameter (ϕ^b) of the residual soil and construction materials for GBS were obtained using the modified triaxial apparatus (Fredlund and Rahardjo, 2003) under consolidated drained (CD) condition following ASTM D7181-11. The schematic diagram and the configuration of the triaxial apparatus is shown in Figure 21. The apparatus is capable of controlling as well as measuring pore-air and pore-water

pressures in the soil specimen independently by using the axis-translation technique in order to achieve the desired matric suction. The details and procedures of unsaturated triaxial tests can be found in Fredlund et al. (2012) and Fredlund and Rahardjo (1993). The results of the unsaturated triaxial CD tests were interpreted using Mohr circles. The failure envelope sloping at an angle of ϕ' was drawn tangent to the Mohr circles at failure. The failure envelope intersected the shear strength versus matric suction plane at a cohesion intercept, c. The cohesion intercepts obtained at various matric suctions were joined to determine the ϕ^b angle. The unsaturated shear strength parameters of residual soil and the materials used in the construction of GBS are summarized in Table 5.

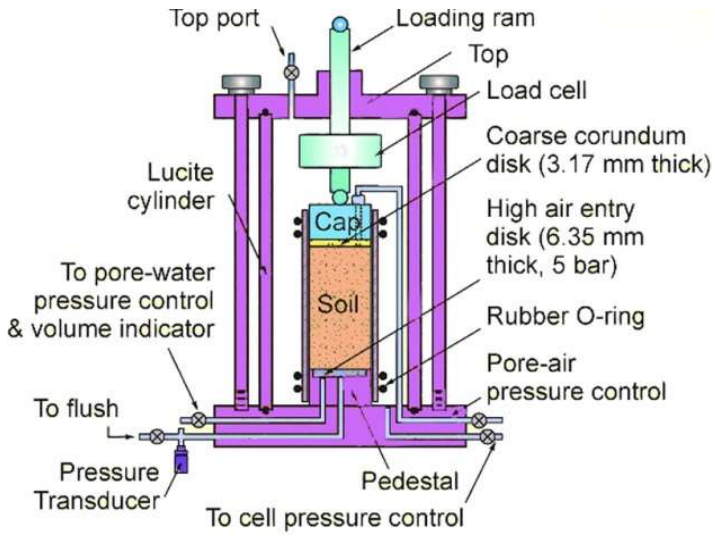

Figure 21: Schematic diagram of modified triaxial cell for unsaturated soil test

Table 5: Shear strength parameters of residual soil and GBS construction materials

Shear strength parameters		Residual soil	ASM	Fine RCA	Coarse RCA	Fine RAP	Coarse RAP	Compacted soil	Gravel
Effective cohesion c' (kPa)		3	2	50	0	0	0	5	0
Effective friction angle ϕ'		35°	30°	42°	47°	36°	32°	37°	42°
Air entry value (AEV)		64	25.65	7.02	0.129	4	0.085	112.5	0.064
ϕ^b	For $(u_a-u_w) \leq$AEV	35°	-	34°	0°	34°	0°	38	-
	For (u_a-u_w) >AEV	14°	-	0°	0 °	0°	0 °	9	-

ϕ^b angle indicating the rate of change in shear strength relative to changes in matric suction, $(u_a - u_w)$.

Construction of Geobarrier System

The pilot study at Orchard Boulevard comprises three GBS slopes and one original slope. In general, the original slope was sloping at 35° to horizontal. Thus, the original slope was excavated for the construction of GBS slope with 70° slope angle. Three GBS slopes were constructed with different combinations of recycled materials as fine- and coarse grained components for CBS (namely GBS slope 1, GBS slope 2 and GBS slope 3). The construction started with the excavation of the original slope to the required dimensions and depth of the GBS slopes. In-situ density tests of the original soil were carried out at three locations (crest, middle and toe of the original slope) prior to the excavation work. Grass and small trees on the surrounding area were removed to avoid hindering the construction work and affecting the performance of the GBS. Reduced levels of all three GBS were maintained the same upon completion of the project. In the event of rainfall during construction, temporary protective canvas covers were used to minimize rainfall infiltration into the slope.

The gravel layer was placed at 1 m depth from the ground surface below the toe of the slope. The gravel was compacted to a relative density between 70% - 90% or to the required dry density of minimum 1.8 Mg/m^3 using a portable compactor. Impermeable separator was installed to separate the gravel below coarse RCA/coarse RAP and fine RCA/fine RAP (Figure 22a). One corrugated and perforated pipe was placed at the end of the gravel layer to drain out the water from coarse RCA/coarse RAP. Three corrugated and perforated pipes were located at the end gravel layer to drain out the water from fine RCA/fine RAP and ASM (Figure 22b). The pipes were connected such that there was only one outlet to the surface drain. All pipes were wrapped with geotextile (Nonwoven Geotextiles TS20) to avoid migration of soil particles that can block the pipe holes. The ASM was placed into the geobag prior to the placement at the designated locations. The fine RCA and fine RAP were also placed into the geobag and compacted into a relative density between 70% - 90% or to the required dry density of minimum 1.55 Mg/m^3. Figure 23 shows the compaction works of fine RCA within the geobag.

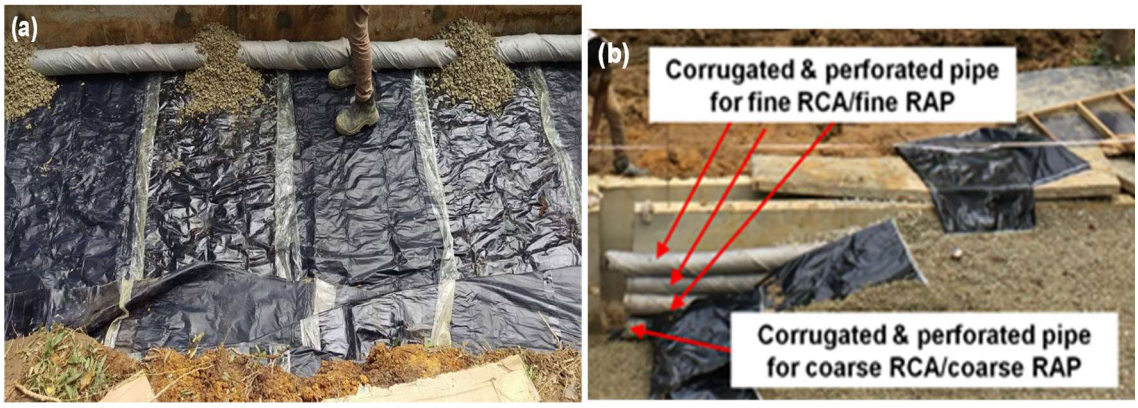

(a) Placement of impermeable layer **(b) installation of perforated drain**

Figure 22: Preparation work and drain installation

Figure 23: Filling and compaction of fine RCA/fine RAP inside geobag

The placement of geobag was carried out in stages. Every stage (500 mm height) was started with the placement of the ASM geobag. The geogrid attached to ASM geobag was stretched up to the maximum length of 2800 mm. Then the geobag for fine RCA/fine RAP was placed behind the ASM geobag (Figure 24a). Prior to the placement of coarse RCA/coarse RAP, the soil up to 1400 mm length behind the fine RCA/fine RAP geotextile bag was compacted to 1.73 Mg/m^3 (Figure 24b). Then, the coarse RCA/coarse RAP was placed in between the fine RCA/fine RAP geobag and the compacted soil (Figure 24c). The coarse RCA/coarse RAP was compacted to the required dry density of 1.8 Mg/m^3.

Figure 24: Construction stages of GBS slopes

In the final stage of the GBS construction (at the crest of the slope), the coarse RCA/coarse RAP was placed directly above the ground surface behind the ASM geobag. Then, geofabric was placed on top of the coarse RCA/coarse RAP before placement of fine RCA/fine RAP. Another geofabric layer was placed before laying ASM layer. Then surface drain was constructed at the back and both sides of the GBS slopes. Vegetations were planted in each pocket of the ASM geobag upon the completion of the GBS slopes. The crest of the GBS slopes were then covered by turfing on the ASM layer. Figure 25 and 26 show the completed GBS and the GBS with green cover, respectively.

Figure 25: Completed GBS slopes at field pilot study site Orchard Boulevard

Figure 26: GBS slopes at field pilot study site Orchard Boulevard after planting

Field Instrumentation

Field instrumentation and monitoring was carried out on the GBS slopes and one section of the original slope to monitor the effect of rainfall on the pore water pressure and slopes deformation. The sensors used in the field instrumentation consisted of rain gauge, piezometers, tensiometers, soil moisture sensors, water flow meter, and earth pressure sensor to measure the slope deformation. All data were collected in a data-logger and transmitted via internet for remote access to enable real time observation The monitoring period was one year commencing on 1st July 2016. The plan view of the slopes and instrumentation locations is presented in Figure 27. The diagram of the GBS slopes and the Original slope constructed for this field study together with the layout of monitoring instruments are shown in Figure 28.

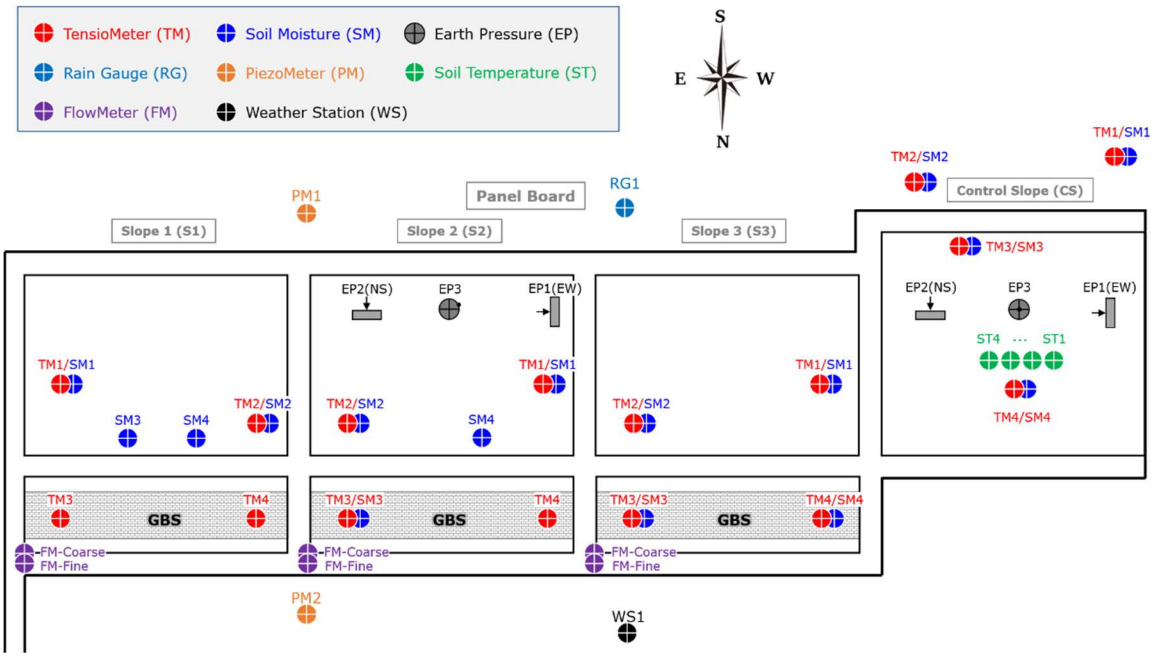

Figure 27: Plan view of slopes at pilot study site with instrumentation locations

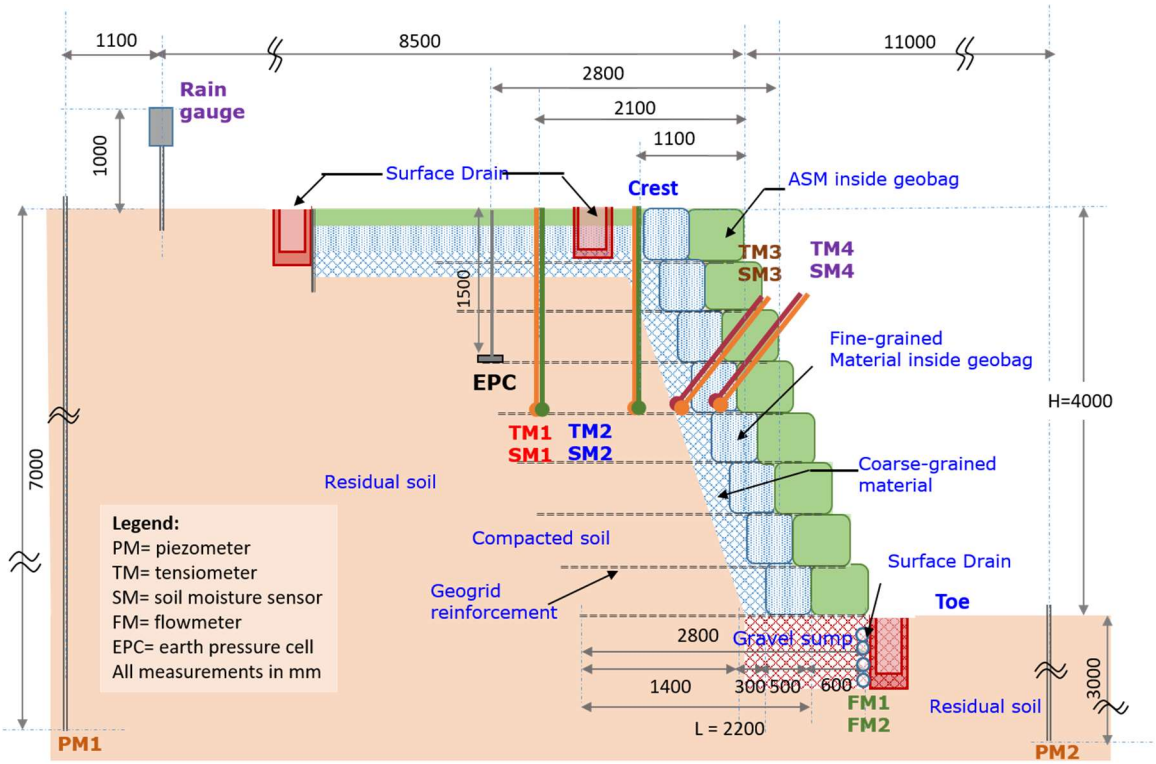

(a) GBS slopes

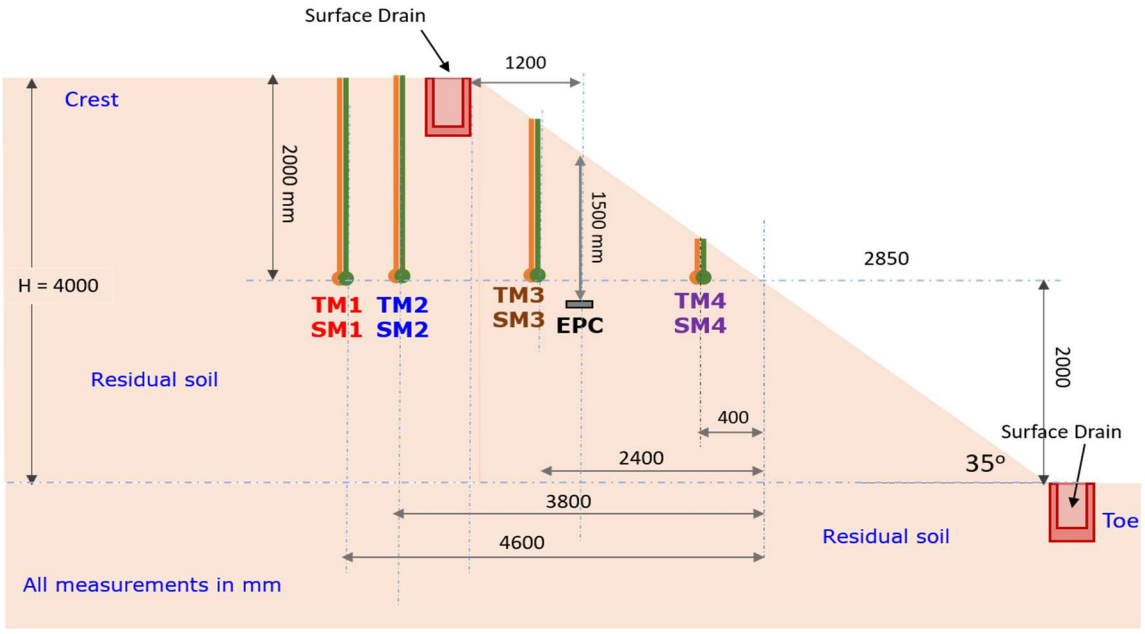

(b) Original slope

Figure 28: Plan view of GBS and original slopes with instrumentation locations

Rain Gauges

The study area was instrumented with a rain-gauge (Figure 29) to monitor rainfall. The rain-gauge was located at 1.6 m above the ground on an open area of the slope crest to determine the rainfall intensity. A tipping bucket rainfall gauge, connected to a magnetic-reed switch, was chosen to collect the rainfall data. Regular maintenance of the rainfall gauge was conducted twice a week as dust and insects might enter the tipping bucket and affected the accuracy of measurement.

Figure 29: Tipping bucket rainfall gauge installed at the study site

Piezometers

The response of groundwater to rainfall was monitored by two piezometers installed at depth of 7 m at the crest and depth of 4 m at toe of the slope. The piezometers, of Cassagrande type (Figure 30) is widely used for groundwater table monitoring in slope because they consist of economical components, simple to read, and have long-term reliability. The piezometer tip was embedded in sand layer that is isolated by two sand bentonite layers. A grout (i.e., mixture of sand and bentonite) was placed into the zone above the bentonite seals to prevent water migration through the zone into the intake area of the piezometer. The fluctuation of groundwater table in response to rainfall was monitored and recorded every week.

(a) Piezometer transducer

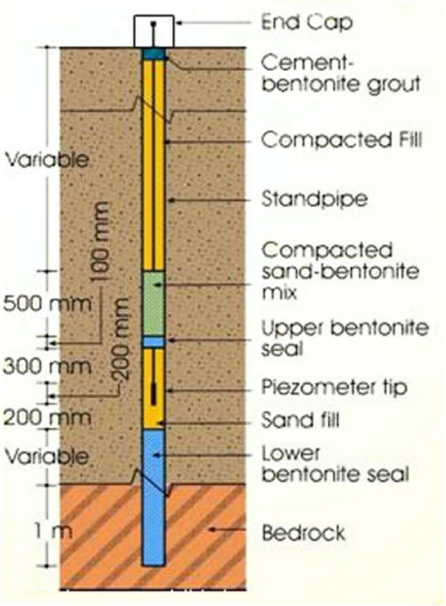

(b) Schematic diagram of Cassagrande Piezometer

Figure 30: Piezometer installed at the study site

Tensiometers

Four tensiometers were installed into the original slope and each GBS slopes to measure pore-water pressure change in response to rainfall infiltration. As shown in Figure 28, all tensiometers in original slopes were installed vertically from crest to a depth of 2 m. TM1 and TM2 of GBS slopes were also installed vertically from crest into compacted soil to a depth of 2 m while TM3 and TM4 were installed from the slope face to coarse and fine layers, respectively. The elevation of TM3 and TM4 from ground surface at crest were also 2 m. Prior to installation, the tensiometers were calibrated properly. Then, each jet-fill tensiometer was inserted inside the tube that has been provided during the construction of the GBS slopes until the tip of ceramic disc was embedded inside the soil. The jet-fill tensiometer (Figure 31) was supported with a bourdon gauge to verify the reading from transducer. The response of tensiometers to pore-water pressure change must be checked regularly to ensure the quality and physical performance of high air-entry ceramic tips. In this study, regular maintenance of the tensiometers was conducted twice a week by refilling the jet-fill reservoir with de-aired water and flushing the tensiometers to remove the accumulated or trapped air in the tensiometer tubes caused by cavitation of water and air diffusion through the ceramic tip.

Figure 31: Jet-fill tensiometer with transducer used in this study

Soil Moisture Sensors

The soil moisture sensor model M406 used in this study was of TDR type which was capable of measuring soil moisture up to saturation (0–100%) with accuracy of 1% and response time of 0.5 second. All soil moisture sensors were tested in water and air environment and their values corresponded to the values specified by manufacturer which was about 70 to 90% in pure water and zero in air. Figure 32 shows the soil moisture sensor and installation of the moisture sensors used at the pilot field study at Orchard Boulevard.

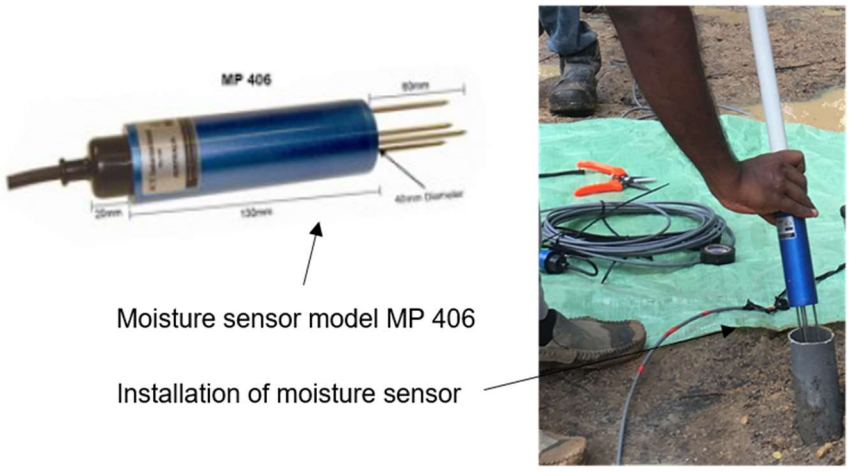

Figure 32: Soil moisture sensor used in this study

Earth pressure cells

Earth pressure cells were installed behind the original slope and GBS slope 2 to monitor the total vertical and lateral stresses changes due to rainwater infiltration in three directions z (i.e., vertical direction), x (i.e., east-west direction: perpendicular to the inclination of the slope) and y (i.e., north-south direction: parallel to the inclination of the slope). The installation of the earth pressure cells was carried out carefully to minimise soil disturbance due to the excavation of the slot for a pressure cell. Figure 33 shows the earth pressure cells installed in GBS slope 2.

Figure 33: Installation of Earth pressure cells in GBS slope 2

Water Flow sensors

Six submersible hydrostatic level transmitters were installed at GBS slopes to monitor if there was a breakthrough to coarse grained layer in the capillary barrier system.

Each slope was served by two flowmeters, one monitored water flowing out from the fine-grained layer and the other monitored if there was water coming out from the coarse-grained layer. The flowmeter used in this pilot study is shown in Figure 34.

(a) Submersible Hydrostatic level Transmitter model 3400

(b) Installed flow meter in GBS slope 2

Figure 34: Flow-meter installed below GBS slopes

On-line Monitoring System

The measuring instruments were calibrated in laboratory and checked on-site prior to installation, to obtain reliable readings. Readings of each instrument (tensiometers, soil moisture sensors, earth pressure cells, piezometers, rain-gauge) were checked before they were connected to a data acquisition system (DAS) to obtain instrumentation readings in real time. The data logger was powered by solar panel and battery. The cables were protected by corrugated tubing to prevent damages from rainfall and insects. The data logger recorded readings at a 10-minute interval regardless of rainfall events. Figure 35 shows the data acquisition system used at the pilot study site at Orchard Boulevard.

All instrumentation readings were sent out to an on-line central server automatically through a communication system that was always connected. At the central server, an automatic computer system converted the monitoring data into engineering values and uploaded the information to a dedicated web page. A web page named "Geo-Barrier at Orchard" was created for the on-line monitoring of data from Orchard Boulevard site. The data logger sends all data to server (PC) using general packet radio service (GPRS) system. GPRS sends the data using a modem installed with the data logger to "Geo-barrier at

Orchard" web page. The web page contains data presented in the time-history plots and other necessary charts for easy reference by the users.

Figure 35: Data acquisition system used at the study site

Field Monitoring Data

Rainfall Records

Figure 36 shows daily rainfall recorded from 1 July 2016 to 30 June 2017. The cumulative yearly rainfall was 2819 mm which is higher than the average annual rainfall in Singapore based on long term record (1869-2016) i.e. 2328.7 mm. The number of rainfall days during the monitoring period was 178 days which is the same as the average annual number of rainfall days in Singapore. Singapore's climate is characterized by two monsoon seasons i.e. The Northeast Monsoon occurs from December to early March with wet periods in December and January followed by dry and windy period from late January to earlier March; and the Southwest Monsoon from June to September with short duration showers/thunderstorms in the afternoon. Rainfall monitoring at Orchard Boulevard indicates that the monthly rainfalls are quite different from the typical trend in Singapore. For example, the monthly rainfall in December 2016 (214.3 mm) was too low as compared to the average rainfall in Singapore for December (> 300 mm). On the other hand, the

monthly rainfall in May 2017 (331 mm) was very high as compared to the average rainfall in Singapore for May (>200 mm). The monthly rainfall in September, October and November 2016 are higher than the average monthly rainfall for the months in Singapore. This inter-monsoon period in Singapore is usually wetter than March – May. Maximum daily rainfall occurred during the monsoon period in January 2017 i.e. 103.8 mm. The month of January 2017 started with a dry period for about two weeks but very wet period towards the end of the month. November 2016 was the wettest month during the monitoring period with cumulative rainfall of 311.3 mm rain and 21 rainfall days while August 2016 was the driest month with cumulative monthly rainfall of 98.6 mm. The highest cumulative rainfall occurred in May 2017 i.e. 331 mm with only 14 days of rainfall.

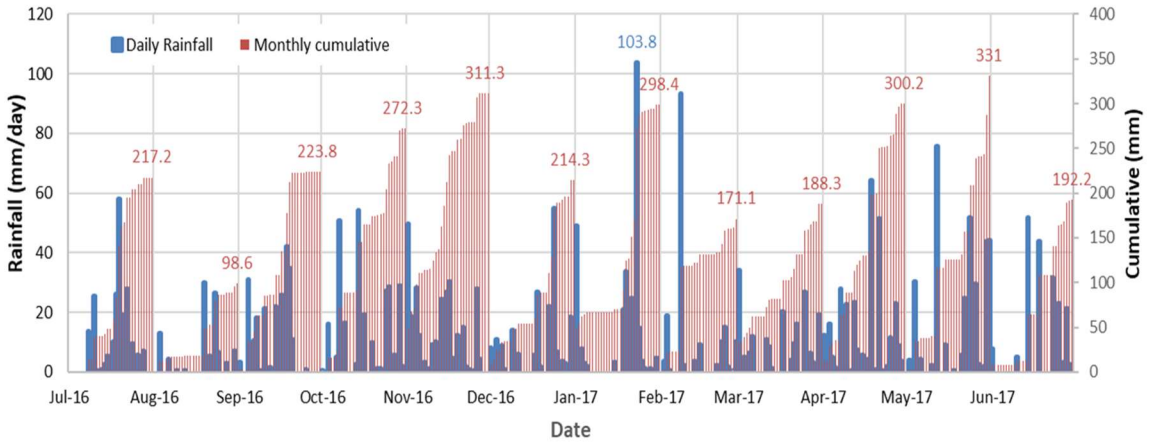

Figure 36: Daily and monthly cumulative rainfall from 1st July 2016 to June 2017

Response of groundwater to rainfall

Figure 37 shows the effect of rainfall on groundwater table fluctuation recorded by piezometer 1 (PM1) and piezometer 2 (PM2) installed near crest and toe of the slopes respectively. The initial groundwater table recorded by PM1 was -6.05 m with reference to the ground surface at the crest while PM2 recorded a groundwater table at -2.37 m with respect to the ground surface at the toe. The highest groundwater table during the field monitoring was -4.37 m below the ground surface at the crest (PM1) and -0.44 m below the toe while the lowest was -7.16 m below crest and -3.33 m below ground surface at the toe (PM2). The groundwater table at the toe rose above the base of gravel sump (-1.00

below ground surface at the toe) a few times during the monitoring period, thus affected the reading of flow meter. The difference on the elevation at crest and elevation at toe is considered in Figure 37. It is shown that the groundwater table below the slopes at the pilot study site was almost flat with an average fluctuation of 2.8m. Figure 38 shows the highest and lowest ground water table during the monitoring period.

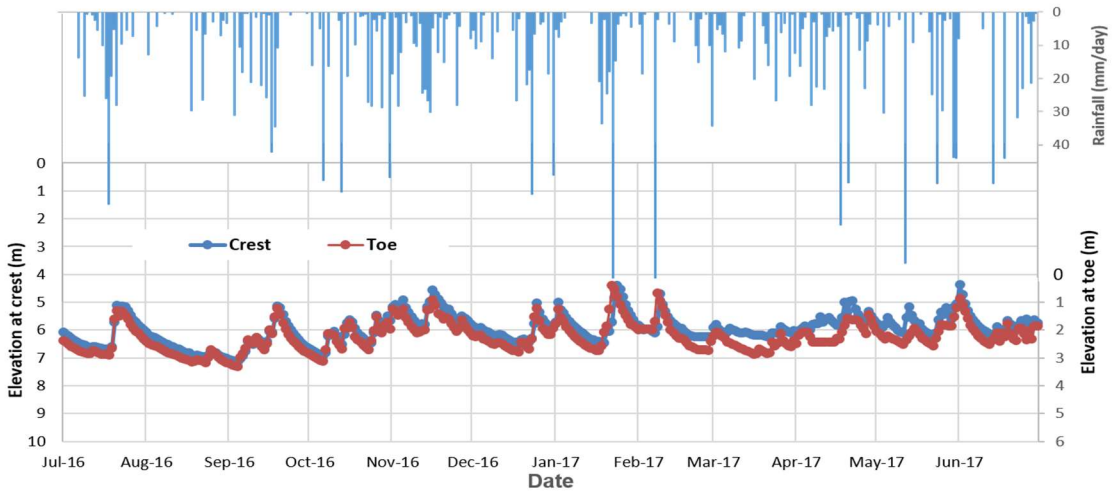

Figure 37: Groundwater table fluctuation in response to rainfall infiltration

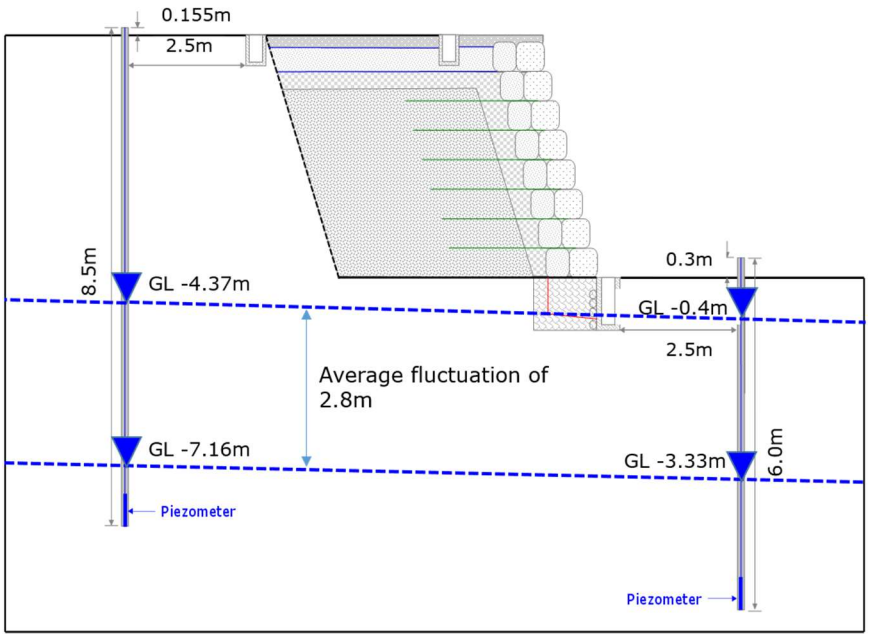

Figure 38: Highest and lowest ground water table during the monitoring period

Pore-water pressure response to rainfall infiltration

As mentioned earlier, three GBS slopes and one section of the original slope were instrumented with tensiometers to observe the response of the slopes to rainfall infiltration in terms of pore-water pressure. Figure 39 shows the pore-water pressure response of GBS slopes to rainfall. The figure indicated that there was not much variation of pore-water pressure recorded in the GBS slope 2. The pore-water pressure recorded by TM1-GBS2 (2.1m from slope face) only varied between 15 and 25 kPa while TM2-GBS2 (1.1 m from slope face) recorded almost constant values. The pore-water pressure in Coarse RAP (TM3) was always constant with time while the readings from TM4 (fine grained layer) fluctuated slightly. On the other hand, the variation of pore-water pressure readings in TM2 of GBS slope 1 and TM1 of GBS slope 3 were quite significant. During long dry period, the pore water pressure could reach -80kPa but the reading recovered as soon as rain started to fall. This could be due to the effect of uneven compaction in the soil. Even-though the pore-water pressure in the compacted soil of GBS slopes 1 and 3 decreased to -80 kPa during dry periods, the pore-water pressure never increased to higher than -15 kPa during rainfall. This means that the change in the pore-water pressure was only due to the change in the moisture content of the soil and rainfall did not actually seeped into the compacted soil. The pore-water pressure readings of TM1 of GBS slopes 1 and TM2 of GBS slope 3 were similar with readings of TM1 and TM2 of GBS slope 2.

Figure 40 shows the response of tensiometers installed in Original slope to rainfall on average daily basis. All tensiometers in the original slope recorded change in pore-water pressure in response to rainfall infiltration. The tensiometers were installed at horizontal distances of 0.4 m (TM4), 2.4 m (TM3), 3.8 m (TM2), and 4.6 m (TM1) from slope face at depth of 2 m. The response of TM4-OS at distance of 0.4m is very significant due to long dry period and high air temperature in December 2016 and early January 2017. The response was more significant as the distance of tensiometer is closer to ground surface. With the exception of this period, the pore-water pressure in all tensiometers varied from -5 to -25 kPa throughout the monitoring period.

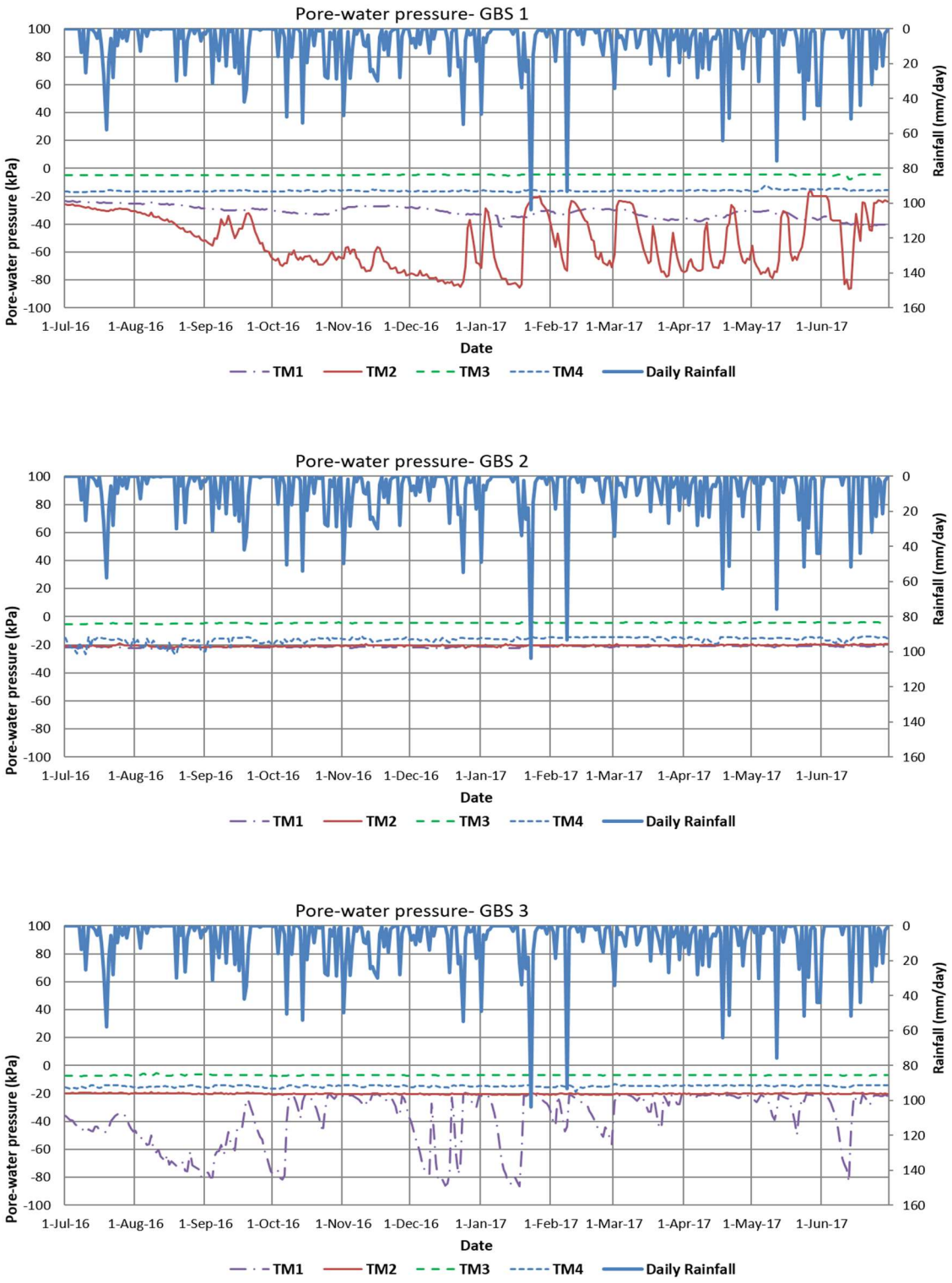

Figure 39: Pore-water pressure readings in the GBS slopes at pilot study site

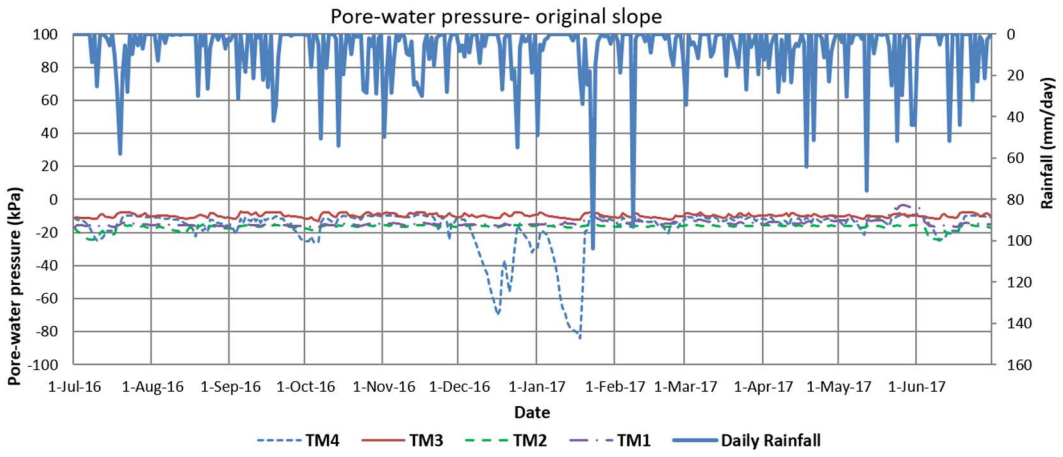

Figure 40: Pore-water pressure readings in original slope at pilot study site

The pore-water pressure readings from the GBS slopes were compared to the readings from the original slope, to identify the performance of the capillary barrier in limiting rainfall infiltration to soil. Comparison of the pore-water pressure variations presented in Figures 39 and 40 supports that the capillary barrier performed well in maintaining the negative pore-water pressure (suction) in the compacted soil. The pore water pressure recorded in the original slopes was higher than those recorded in the compacted soil within the GBS slopes. The pore-water pressure measured by TM3 in coarse grained layer was always constant, meaning that the rainfall did not infiltrate into this layer. The pore-water pressure in the fine grained layer fluctuated with rainfall but never reached zero indicating that the layer was affected by rainfall but the water never saturated the fine grained layer. The pore-water pressure measured in original slope varied in response to rainfall. However the variation recorded by TM4, was the most significant. This could be due to the position of TM4 which was closest to the ground surface (perpendicular distance to slope face was 0.23 m), thus readings of TM4 was subjected to the effect of evapotranspiration as well as the ASM soil used to grow the vegetation.

The responses of pore-water pressure and volumetric water content to an individual rainfall were evaluated every week. Figure 41 shows the response of pore water pressure to an individual rainfall on 26th November 2016. The accumulated rainfall during 2 hours

was 27 mm. This rainfall induced more variation in the pore-water pressure readings in the original slope as compared to the pore-water pressure readings in GBS slopes.

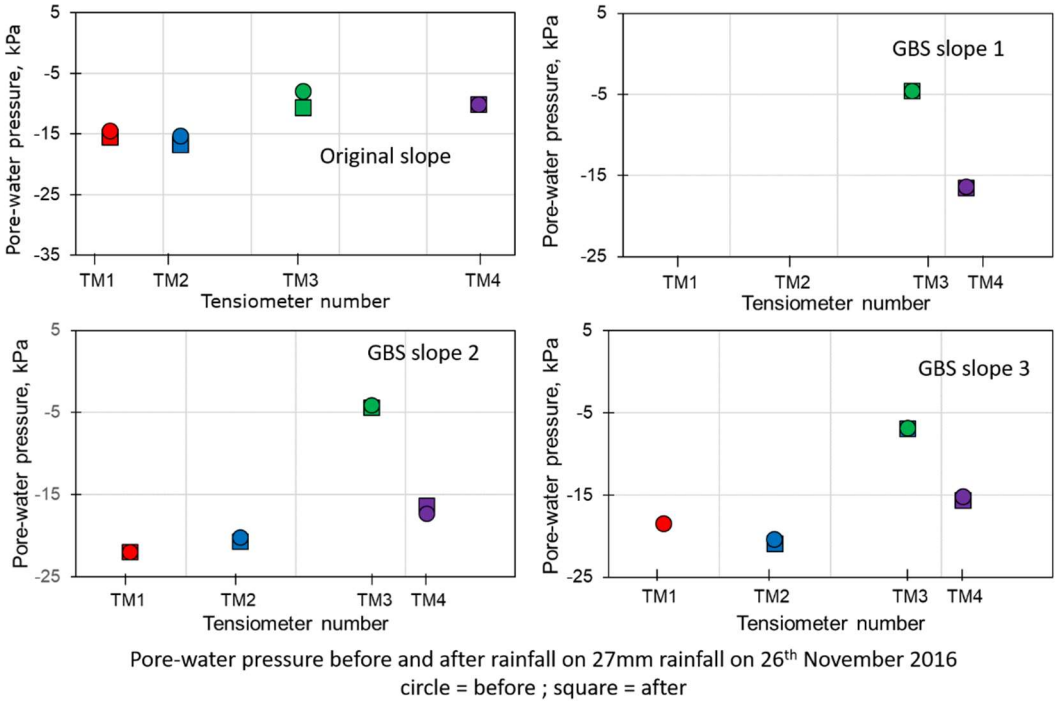

Figure 41: Pore-water pressure response of original and GBS slopes

Soil Moisture response to rainfall infiltration

The soil moisture responses to rainfall infiltration in GBS slopes are shown in Figure 42. In general, the soil moisture in the compacted soil within the GBS slopes (TM1 and TM2) varied from 10 to 35 kPa. The volumetric water content in fine RCA in GBS slope 1 was between 20 to 30% while in GBS slope 3 was about 10%. The volumetric water contents in fine RAP in GBS slope 2 varied between 8 and 20%. The volumetric water contents in the coarse aggregate (RCA and RAP) were lower than 7%. Figure 43 shows the soil moisture response in the original slope. The volumetric water content in the residual soil forming the original slope varied from less than 10% to 55%. This variation was more significant than that in the GBS slope. This supports that the capillary barrier played its role to prevent rainwater to infiltrate into the coarse grained layer as well as the reinforced soil. The soil moisture readings at GBS slope were almost constant with time except in the fine-grained layer, meaning that the rainfall did not infiltrate into these layers.

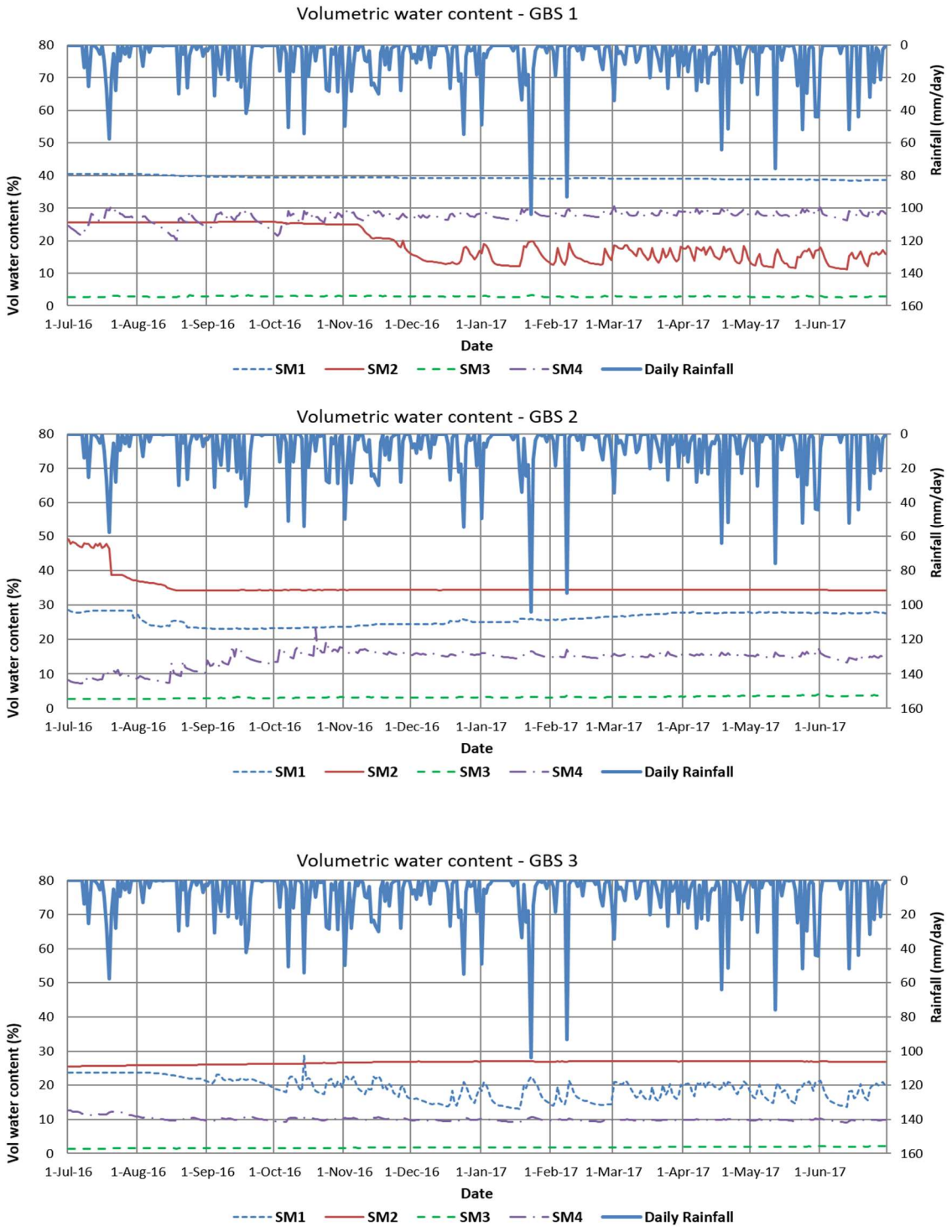

Figure 42: Volumetric water content readings in the GBS slopes at pilot study site

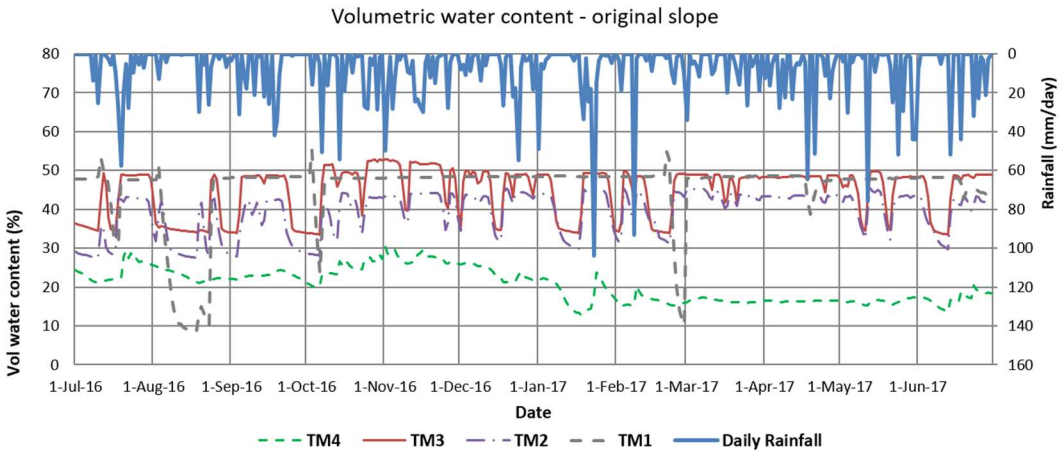

Figure 43: Volumetric water content readings in original slope at pilot study site

Figure 44 shows the response of volumetric water content to the individual rainfall on 26th November 2016. Similar with the pore-water pressure readings shown in Figure 41, the 27 mm rainfall induced changes in the volumetric water content readings in original slope. The effect of rainfall on the volumetric water content readings in the original slope was more than the effect on GBS slopes.

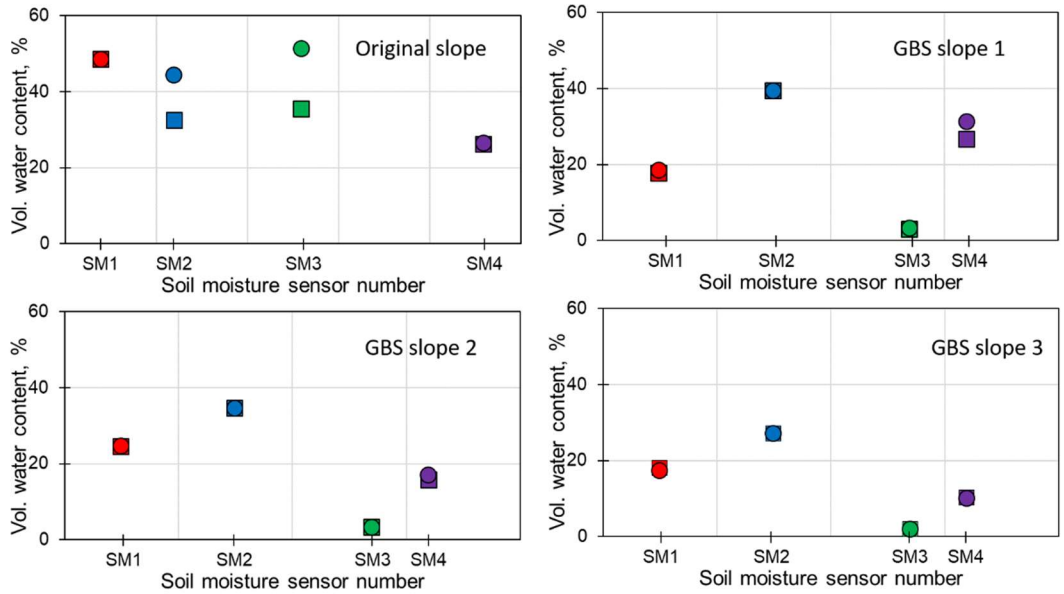

Figure 44: PWP and VWC response of original slope and GBS slopes

Field verification of SWCC curves

The field data on pore-water pressure and volumetric water content were plotted on SWCC curves of the respective materials i.e. (a) residual soil; (b) the compacted residual soil; (c) coarse RCA from GBS slope 1 and fine RCA from GBS slope 1 and GBS slope 3; and (d) coarse RAP from GBS slope 2 and 3 as well as fine RAP from GBS slope 2. As shown in Figure 45, the field data from TM1-SM1; TM2-SM2; TM3-SM3 in the original slope were plotted well inside the hysteretic loop of drying and wetting curves of residual soil. This means that the SWCC obtained from laboratory test is representative of the SWCC of residual soil and can be used for numerical analysis. However, readings from TM4-SM4 were plotted below the wetting curves, thus not shown in Figure 45. It is thought that because the position of TM4-SM4 was very close to ground surface (0.23m perpendicular distance from slope face), the readings were influenced by evapotranspiration. Besides, the response of TM4-SM4 at this position was affected by the behavior of ASM used for growing the vegetation.

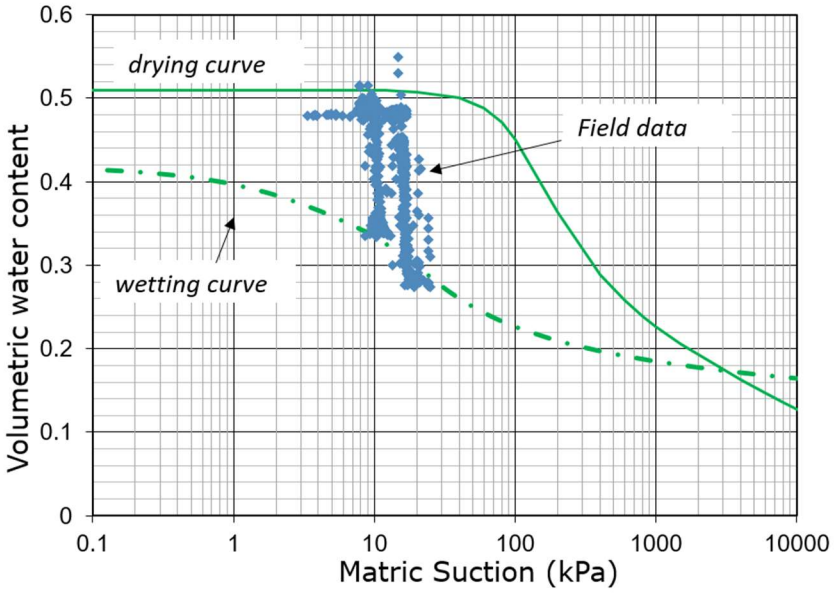

Figure 45: Plot of Field measurements in original slope on SWCC of residual soil

Figure 46 shows the plot of field data on compacted soil in GBS slopes 1, 2 and 3. This figure also shows that all field data fall within the hysteretic loop of drying and wetting curves of the compacted residual soil. The plot of field data in coarse and fine materials forming the capillary barrier of GBS slopes are shown in Figure 47 and 48. Most field data for coarse materials (RCA and RAP) are in the residual part of the SWCC. This is due to the condition of coarse RCA during construction was dry. Rainwater did not infiltrate into the coarse RCA, thus maintaining the dry or residual condition. The field data on fine materials (RCA and RAP) varied more significantly in terms of volumetric water content. For fine RCA, the data was concentrated in the transition zone of SWCC drying curve. Lower volumetric water contents were recorded in GBS slope 3. For fine RAP, the data concentrated toward the residual zone of SWCC due to the initial condition RAP.

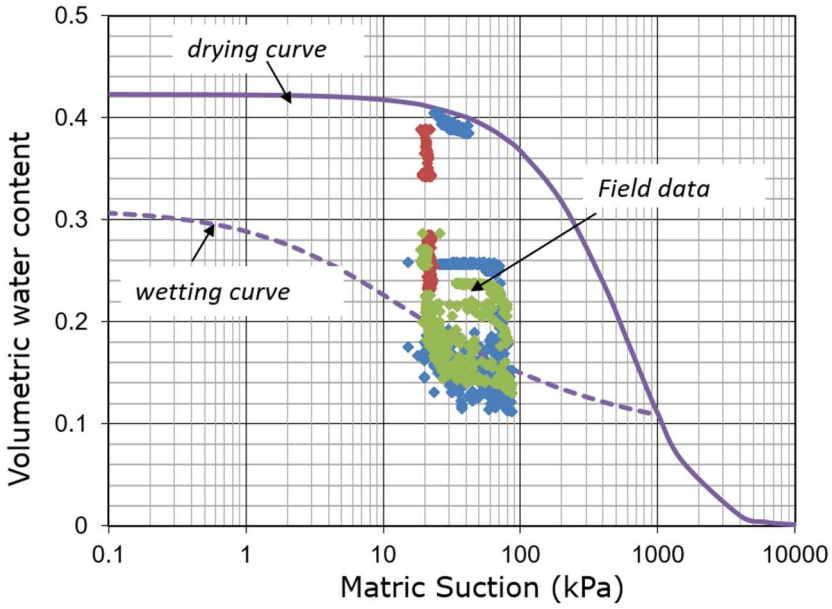

Figure 46: Plot of Field measurements in GBS slopes on SWCC of compacted soil

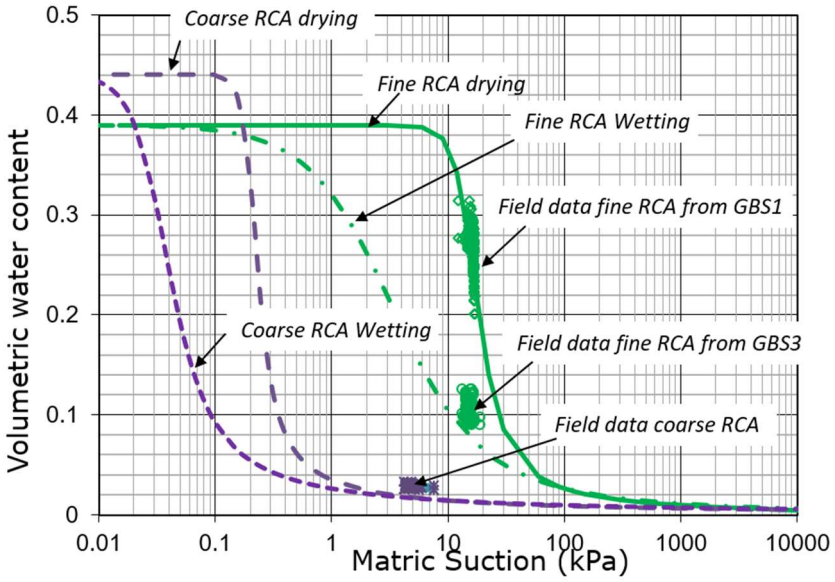

Figure 47: Plot of field measurements in GBS slopes on SWCC of RCA

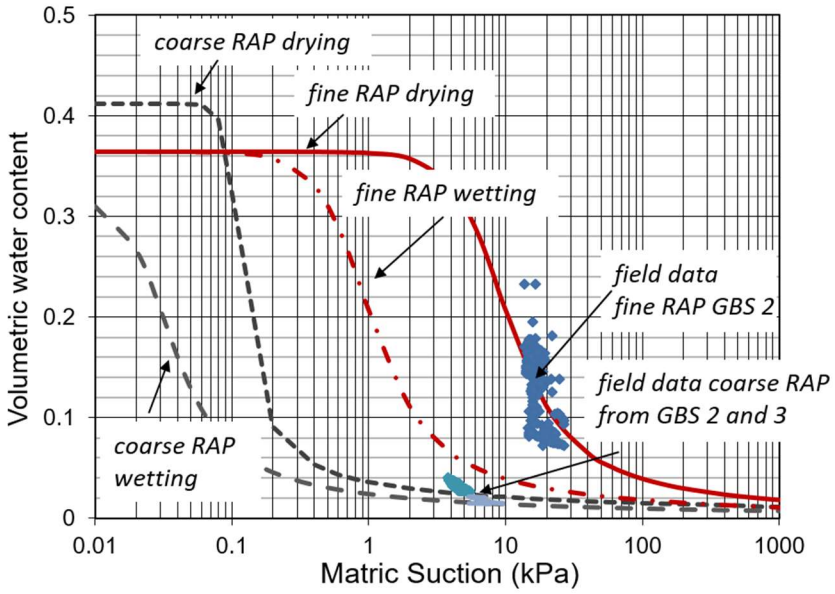

Figure 48: Plot of field measurements in GBS slopes on SWCC of RAP

Water Flow from fine and coarse-grained layers

Flow meters were installed inside the sump located below the GBS slopes to measure any flow from fine and coarse grained layers. In addition, flow-meters are required

to observe if there was a breakthrough from fine grained layer to the coarse grained layer. One year monitoring shows that the flow meters did not record any flow from both layers. However, the flow-meters recorded some flows at times when the ground water level rises to a depth of less than 1 m below ground surface. This shows that rain water mostly became run off or was absorbed by ASM layer.

The infiltration characteristics of fine material was evaluated by field infiltration test conducted prior to the decommissioning of the site. In this test, 2000 litre of water was streamed directly to the fine-grained layer by digging a ditch at the crest. The responses of tensiometer, moisture sensor and flow meter were monitored. No water flow from fine-grained layer was monitored until the end of test. However there was variation in pore-water pressure and volumetric water content recorded by TM4 and SM4 in the fine layer at depth of 2 m from crest. No change in pore-water pressure and volumetric water content was recorded by TM3 and SM3 in the coarse-grained layer. This indicated that there was no breakthrough in the CBS even after a large amount of water was flowed through the fine grained layer.

Earth pressure response to rainfall infiltration

While all slopes were instrumented with tensiometers and soil moisture sensors, only GBS slope 2 and original slope were also instrumented with earth pressure cells. The cells were installed at depth of 1.5 m from the ground surface at the crest. Earth pressure variations in the original slope and GBS slope 2 are shown in Figure 49. The figure indicated that the vertical pressures (z- direction) recorded in both GBS slope 2 and the original slope are equivalent to the theoretical value assuming the density of the soil was 1.8 Mg/m^3. The vertical earth pressure recorded in GBS slope was less affected by rainfall than that recorded in the original slope. In the original slope, the horizontal pressure in y-direction started at a value lower than in the x-direction but with time, the values became closer. On the other hand, in GBS slope 2, the horizontal pressures were similar in x- and y- directions but the pressure in y-direction increased more significantly with time. The horizontal pressure in both y- and x-directions increased in the wet period and was remained constant during dry period.

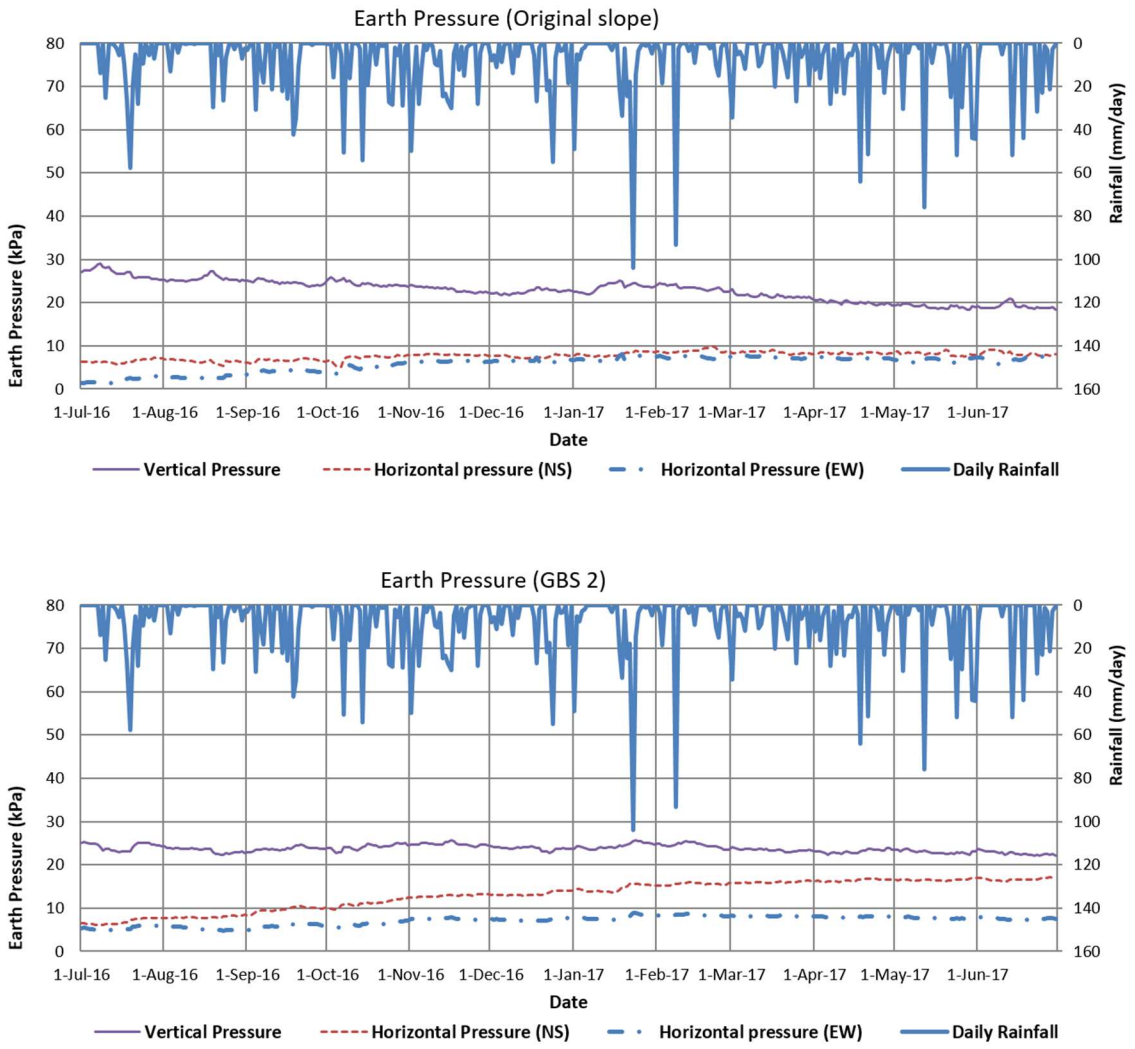

Figure 49: Earth pressure variation in original slope and GBS slope 2

Weekly monitoring indicated that individual rainfall caused an immediate increase of vertical and horizontal pressure but the stress increase was released after a while. Figure 50 shows the response of earth pressure readings to individual rainfall on 26th November 2016. The immediate pressure increase in both original and GBS slopes was believed to be due to the accumulation of water on crest and ASM layer of GBS before it was drained. Figure 50 shows that the immediate pressure increase in GBS slope is less than the increase in the original slope.

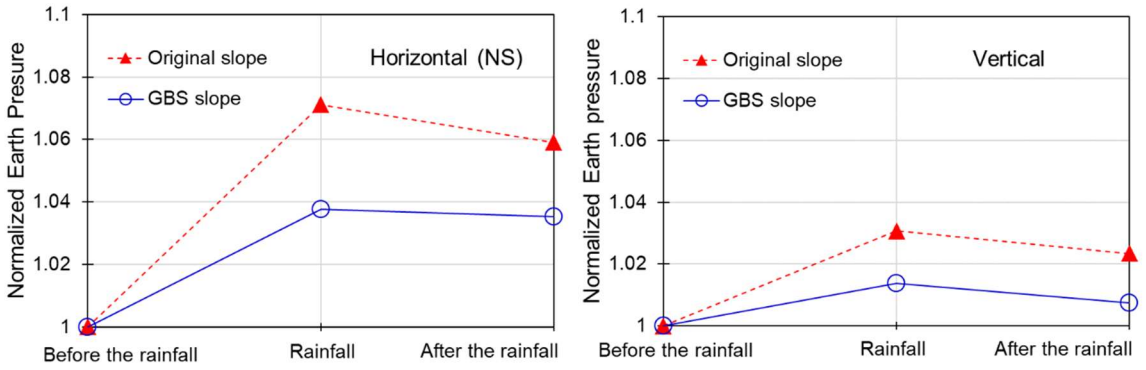

Figure 50: Earth pressure responses to rainfall on 26th November 2016

Overall trend indicates that the vertical pressure increased slightly during the wet period and decreases slightly during the dry period and horizontal pressure (NS or crest to toe direction) in GBS slope 2 increased more markedly than the vertical pressure. This could be due to the response of the soil to construction activity. Pressure changes caused by the construction activity induced an active condition but the slopes will eventually be back to "at rest" condition; causing the increase in the horizontal pressure. Long time monitoring shows that the rainfall had insignificant effect on both vertical and horizontal pressures in both the original and GBS slope because the variation in pore water pressure and soil moisture content was minimum. Figure 51 shows the total stress ratio in GBS slope 2 in the NS (crest to toe direction) is higher than the ratio in the original slope because the GBS slope is steeper than the original slope.

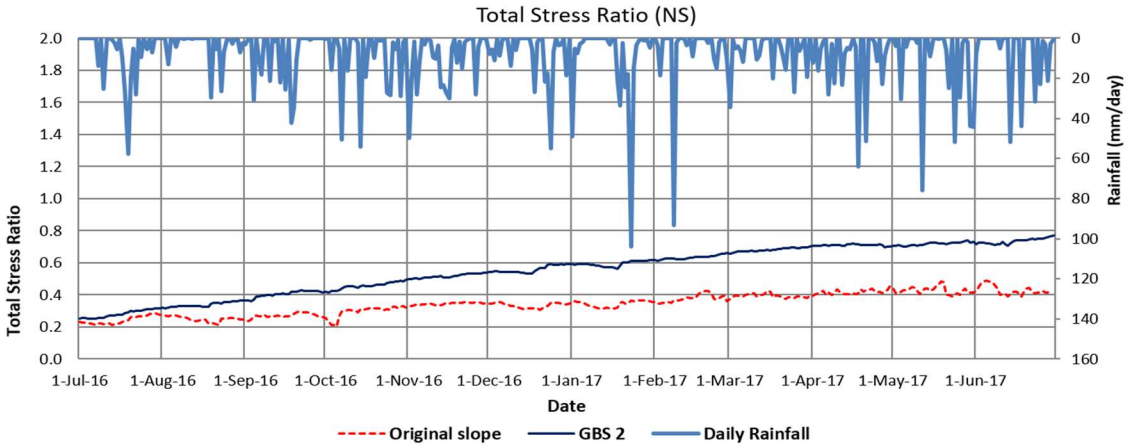

Figure 51: Total stress ratio in original slope and GBS slope 2

Numerical Modelling

Numerical analysis was carried out to model the response of the GBS walls to actual rainfall, thus the performance of the GBS slope could be predicted using the numerical model for different conditions related to soil properties and flux boundary conditions. Deformation-seepage-stability analyses were performed using SIGMA/W and SLOPE/W (Geoslope International, 2012).

Flux Boundary Conditions

The one-year rainfall records shown in Figure 36 indicate that the month of January 2017 could be considered for the numerical analyses because it started with a long dry period, followed by one week of a very wet condition. The rainfall started at 14:20 on 18th January 2017, and the intermittent rainfalls lasted until 23th January 2017. The cumulative rainfall during this one week period was 204 mm while the highest daily rainfall was 103.8 mm on 23rd January. The maximum hourly rainfall was 38.7 mm/h at 10:00 am on 23rd January. The plot of hourly rainfall from 00:00 on 18th January to 23:50 on 23rd January is shown in Figure 52. This rainfall was used as the flux boundary condition in the numerical analysis. Groundwater table and the pore-water pressure within the residual soil behind GBS slope was set as spatial function based on the pore-water pressure measurement at 00:00 on 18th January 2017.

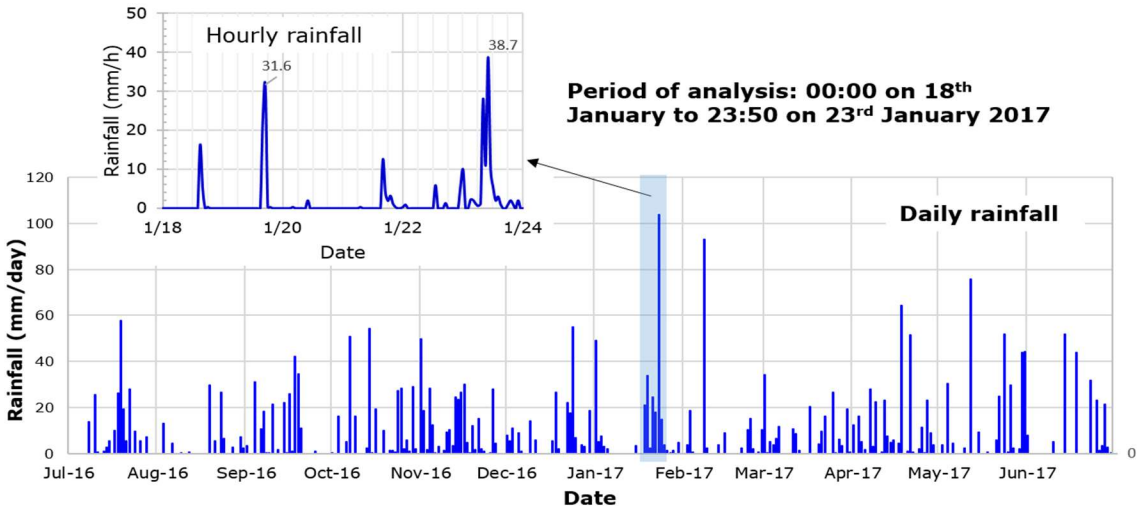

Figure 52: Flux Boundary condition considered in numerical analysis

Finite Element Model

The deformation-seepage analysis was carried out to study the response of the GBS walls subjected to heavy rainfall condition as shown in Figure 52. The mesh and the boundary conditions applied to the finite element model are illustrated in Figure 53. The mesh consisted of 3593 rectangular and triangular elements. The left and right boundaries were set at 10 m and 10.7 m from the crest and toe, respectively. The bottom boundary was set at 8 m from the ground surface at the toe of the slope. For the deformation analysis, zero vertical displacements were assigned at both vertical boundaries and the bottom of the model. For the seepage analysis, no flow boundaries were simulated by assigning a nodal flux Q equal to zero at the bottom and sides of the slope model above ground water level (GWL). A constant total head h_w was applied on each side boundary below GWL. The rainfall was applied to the ground surface as a flux boundary q. Ponding was not allowed to occur on the ground surface, which meant that the PWP was not allowed to be greater than 0 kPa on the ground surface. This condition simulated the actual condition whereby the excess rainwater on the slope would become runoff.

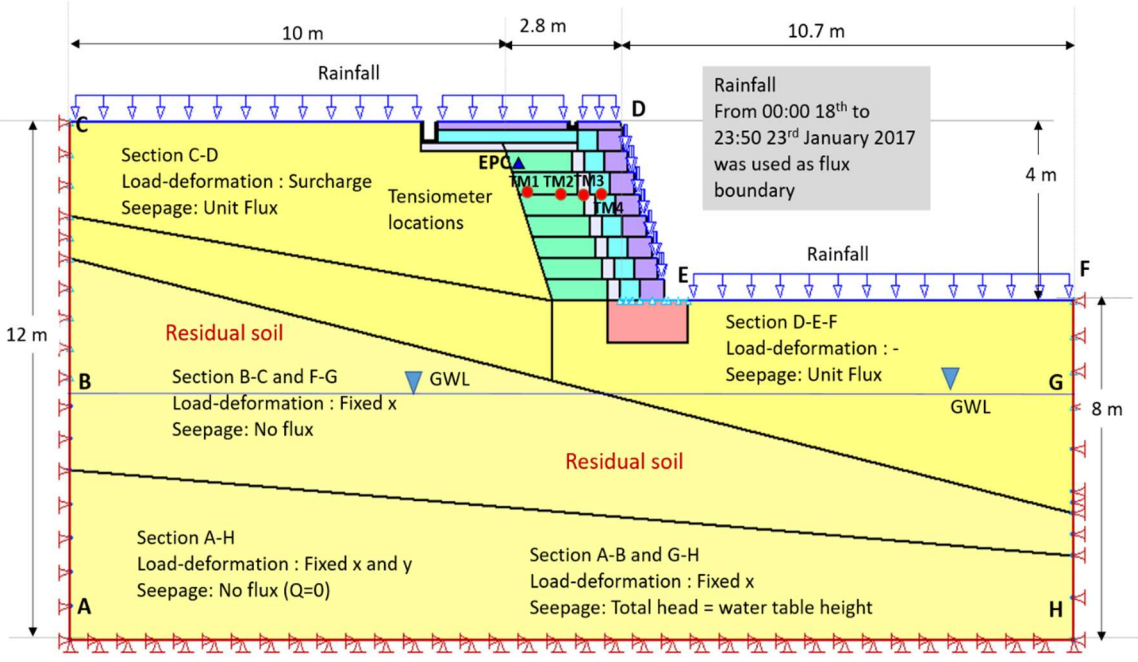

Figure 53: Mesh and boundary conditions for numerical analysis

Material Properties

Three GBS slopes were constructed at Orchard Boulevard. Thus the numerical analysis was carried out on GBS slope 2 which consists of fine RAP over coarse RAP. The soil experiences wetting and drying process due to weather changes, thus the wetting and drying curves serve as boundary of scanning curves of SWCC. Tami et al (2004) showed that the hydraulic properties of the soil in wetting path is more representative for the analysis of rainfall infiltration though the soil, thus SWCC and permeability function in the wetting path, as shown in Figures 54 and Figures 55 respectively, were used for the seepage analysis. The SWCC fitting parameters and the properties of materials used in the numerical analyses are summarized in Table 6. The construction sequence adopted in the numerical analysis started with an in-situ condition and placement of eight lifts of reinforced layers and geobags, followed by the application of rainfall on the ground surface.

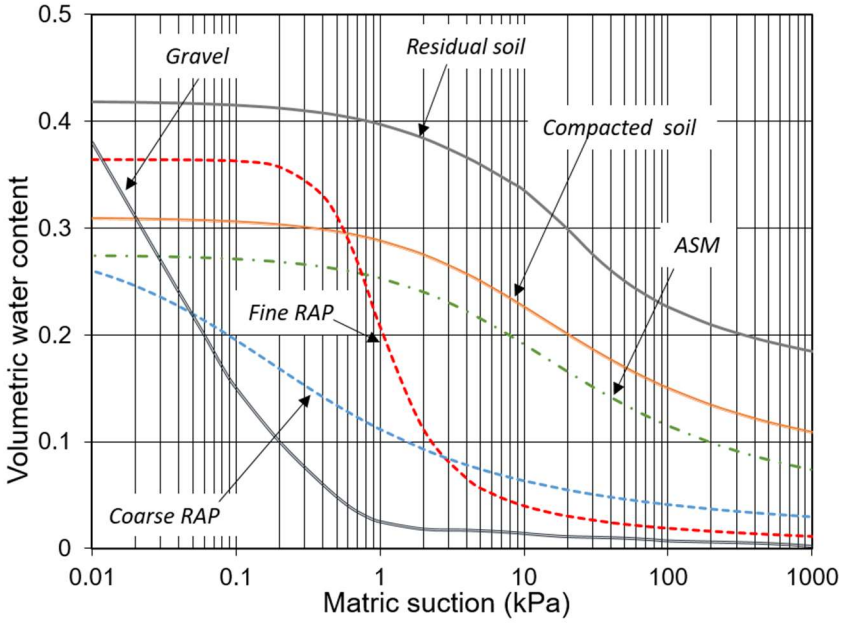

Figure 54: SWCC used for numerical analysis

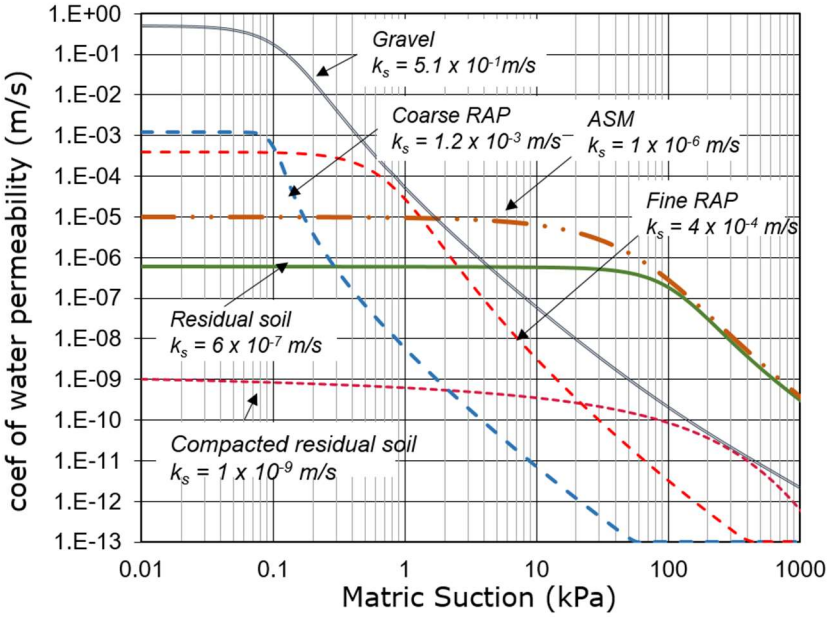

Figure 55: Permeability function used for numerical analysis

Table 6: Hydraulic and shear strength properties of materials for numerical analysis

Description	Symbol (Unit)	ASM	Residual soil	Fine RAP	Coarse RAP	Gravel	Compacted soil
Fitting Parameters of SWCC	*a*	56.11	98.5	7.17	0.098	0.11	1630
	n	1.55	2.6	2.439	9.619	2.72	1.06
	m	0.785	0.41	1.192	0.784	0.79	7
Saturated vol. water content	θ_s	0.381	0.51	0.364	0.412	0.39	0.423
Air-entry value	ψ_a (kPa)	26	64	4	0.09	0.07	112.5
Coef. of saturated permeability	ks (m/s)	1×10^{-5}	1×10^{-7}	4×10^{-4}	1.2×10^{-3}	5×10^{-1}	1×10^{-9}
Shear strength properties							
Effective cohesion	c' (kPa)	2	5	0	0	0	3
Effective friction angle	ϕ' (°)	30	28	34	35	35	38
ϕ^b for $0<(u_a-u_w)\leq \psi_a$	ϕ^b (°)	30	28	34	35	35	38
ϕ^b for $(u_a-u_w) > \psi_a$	ϕ^b (°)	15	17	17	17	17	14
Total unit weight	γ (kN/m^3)	16.5	18.0	15.5	18.0	18.0	20.0

*Air-entry values were computed using Zhai and Rahardjo (2012) equations.

∗ ϕ^b angle indicating the rate of change in shear strength relative to changes in matric suction, (u_a-u_w).

Pore-water Pressure Distribution

The results of the seepage analyses were evaluated at time 0 (before rainfall application i.e. at 00:00 on 18th January) and during rainfall (1-day, 2-day, 4-day) and at

the end of rainfall period (6-day or 23:50 on 23rd January). Figure 56 shows the PWP variations in GBS slope 2 predicted by seepage analysis as compared to the field data. Both results indicate that, even under this heavy rainfall amount, there was very small variations in the PWP in compacted soil as well as in the fine and coarse layers.

In general, the results of numerical analysis agree with the field data except for the PWP recorded by TM1, whereby numerical analysis indicated an increase in PWP after 3 days of intermittent rainfalls while the field data did not show significant increase. The field data suggested that the PWP in the compacted soil was between -18 and -22 kPa while the numerical analysis showed an increase in PWP in TM1 up to -7.2 kPa. This shows that only a small amount of rain-water infiltrated through the GBS slope even under a heavy rainfall condition. The PWPs recorded in the fine-grained material were slightly affected by the rainfall (fluctuated between -14.5 and -16.5 kPa) but the PWPs in the coarse grained layer were almost constant at -4.5 kPa. This indicated that there was no breakthrough under the heavy rainfall from 18th to 23th January. The numerical analysis indicated an increase in PWP in the fine RAP up to -10 kPa and a slight increase in PWP in the coarse-grained layer, with a maximum value of -2.2 kPa.

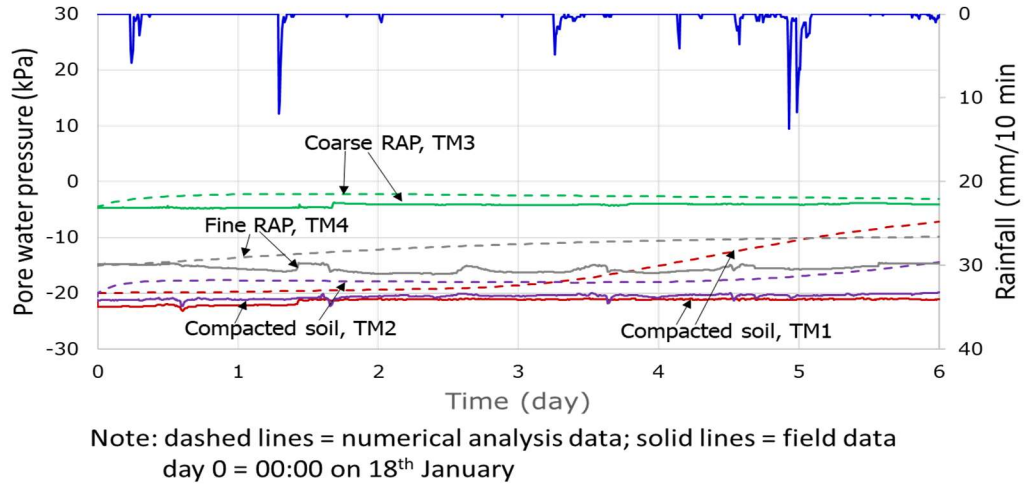

Figure 56: Pore-water pressure variation in GBS slope 2

Earth Pressure Distribution

Figure 57 shows the total vertical and horizontal pressures predicted from the numerical analysis as compared to the monitoring data from the earth pressure cells in GBS slope 2. The figure indicates that the numerical analysis predicted a more significant effect of rainfall infiltration as compared to the field data.

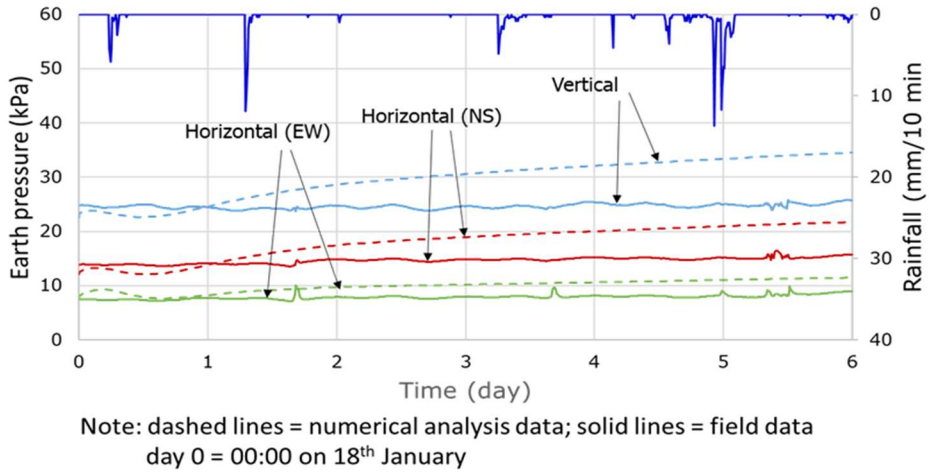

Figure 57: Vertical and horizontal pressure variation in GBS slope 2

Deformation of GBS slope

Figure 58 shows the surface (crest) and face displacement of GBS slope 2 during the period of analysis (00:00 on 18th January to 23:50 on 23rd January 2017). The patterns indicated that the movement of the near vertical slope started at the bottom indicating that the stage construction induced a settlement on the crest and the movement was transferred to the lower part of the slope. Maximum displacement at this stage was only 7.5 mm at the surface and 4.5 mm at the lower part of the slope. Rainfall induced a swelling on the crest on the first two days but then the elevations were back to the original position at the end of analysis period because the top of the slope face started to move horizontally. Maximum displacement of slope face (11 mm) was achieved at the end of analysis period. At this stage, the slope face moved almost the same amount. The relative displacement on top of the slope indicates that part of the rain water was stored in the ASM layer, inducing an increase in the soil mass, thus larger movement at the top. This also explain the increase in

the horizontal pressure recoded by earth pressure cell in NS direction (Figure 49) which is located in the upper part of the slope. As the water in ASM layer seeped downward, the movement of the slope face became more uniform. The water movement in the ASM layer influenced the deformation of the wall.

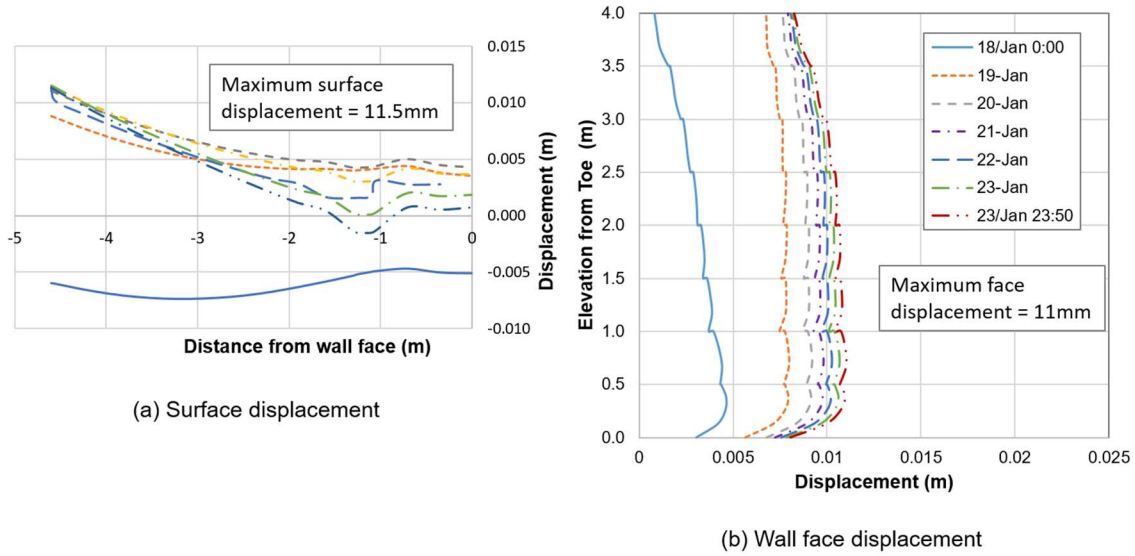

Figure 58: Displacement of GBS slope 2 due to rainfall infiltration

Slope Stability

Slope stability analysis evaluated using limit equilibrium method using SLOPE/W (Geoslope International, 2012) using the pore-water pressure conditions at time 0 (before rainfall application), during rainfall (1-day, 2-day, 4-day) and at the end of rainfall period (6-day or 23:50 on 23rd January). The slope stability analyses were carried out for two possible slip surfaces i.e. global failure of the wall whereby the whole system will slide along the slip surface below the GBS, and local failure in which the slip surface will form inside the GBS itself. Figure 59 shows the variation of factor of safety with respect to the local and global slip surfaces shown in Figure 60a and 60b, respectively. Figure 59 indicates that the local stability of the GBS was not affected by rainfall infiltration because the system is protected by capillary barrier. The global stability was slightly affected by the rainfall because rainfall infiltration induced an increase of pore-water pressure and possible rise of GWL. However, the global factor of safety of at the end of rainfall was still

high (i.e. 2.35). The initial GWL in the pilot study site was quite shallow i.e. at a depth of 2.8m below the toe at 00:00 on 18th January 2017 and it raised to 0.7m below the toe due to the heavy rainfall on 18th to 23rd January 2017.

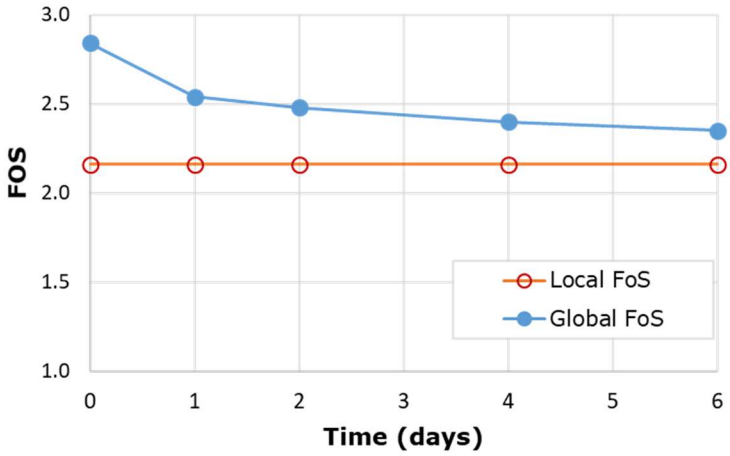

Figure 59: Variation of Factor of safety of GBS slope calculated by SLOPE/W

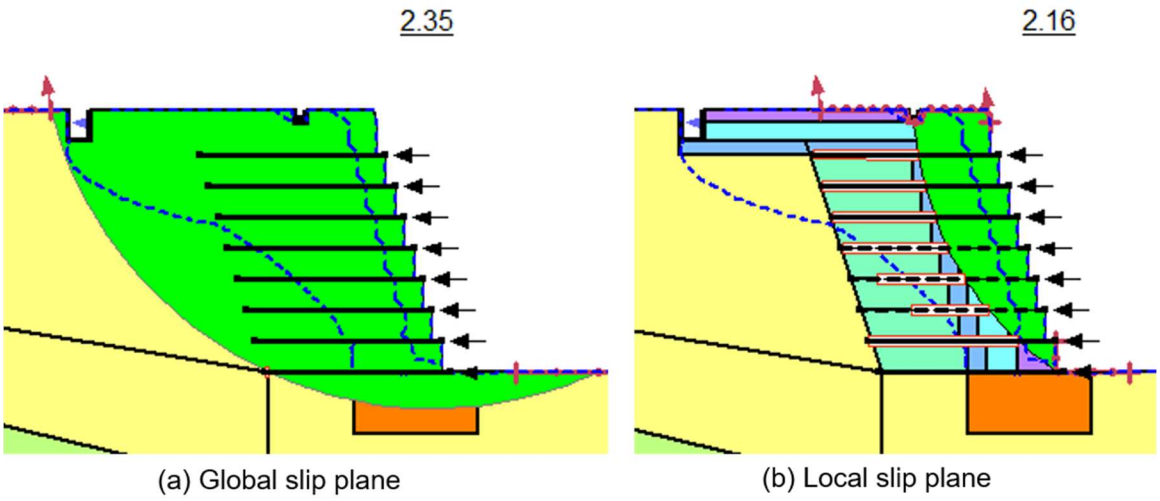

Figure 60: Failure planes developed in GBS slope 2

Tensile Stress in Geogrids reinforcement

The maximum tensile stress developed in the geogrids could be determined from slope stability analysis using SLOPE/W based on the pull-out force developed along the local slip plane shown in Figure 59b. Since the pore-water pressure within the reinforced fill did not change due to rainfall, and the factor of safety as well as the slip plane within the GBS body did not change, then the tensile stress developed in the geogrids reinforcement was not affected by rainfall. This means that the increase in the horizontal pressure recorded by both field measurements and numerical analysis did not translate to the stress mobilized in the geogrids. The maximum tensile force developed in each geogrids layer throughout the analysis period is shown in Figure 61. It can be seen from this figure that the maximum tensile force (11.28 kN/m) was sustained by the second and third layer from bottom (1.5 m from ground surface). This is lower than the allowable tensile stress of geogrids calculated based on the initial characteristics of the geogrids used for the construction of the GBS slopes divided by the combined factor of safety (i.e. 30 kN/m/1.67 = 17.96 kN/m). Field pull-out test, performed on site prior to the decommissioning of the site, indicates that the average pull-out force was 14.55 kN/m, higher than the numerical prediction but still lower than the allowable tensile capacity of the geogrids.

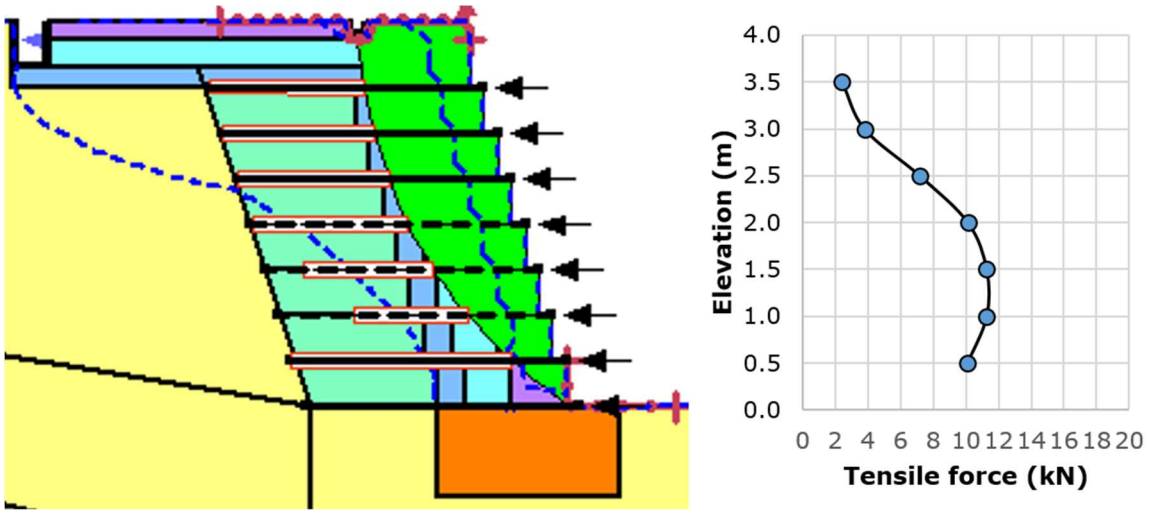

Figure 61: Maximum tensile force generated in each geogrids layer

Conclusions

The following conclusions are drawn from laboratory experiments, field study and numerical analyses:

1. The results of all laboratory tests supported that the materials selected for the construction of the GBS in the pilot study are suitable for the intended purposes. The recycled materials do not contain any harmful substances that can negatively affect the environment. The combinations of fine- and coarse-grained materials derived from the recycled material are suitable to be used as components of the capillary barrier system. Furthermore, the ASM has a good quality as the planting soil. The ASM placed on top of fine-grained layer can act as moisture retention layer.
2. Field monitoring at pilot study site shows that the GBS is effective as a slope protection from rainfall induced instability. The suction measured in the coarse-grained layer as well as in the compacted soil in GBS slope at Orchard Boulevard remained constant despite high intensity and long duration rainfall. The suction in fine grained layer fluctuated with rainfall but the layer never reach full saturation. This shows that most of the rain water became run-off or was contained in the ASM and directly drained into the gravel sump instead of infiltrating into the fine-grained layer. This observation was supported by the results of field infiltration test conducted after the completion of the monitoring period. Observations of the pore-water pressure were supported by the observation on moisture content. The range of pore-water pressure and volumetric water content measured during the monitoring period plotted well inside the hysteretic loop of the drying and wetting SWCC of most materials.
3. Numerical analysis using coupled deformation seepage analyses showed that the effect of rainfall infiltration into the reinforced soil in the GBS wall was minimum because it was protected from rainfall infiltration. The pore-water pressure in the reinforced (compacted) soil remained constant despite being subjected to the extreme rainfall on 18th to 23rd January 2017. The pore-water pressure variations predicted from the numerical analyses agree with those from field data.

4. Deformation analysis indicated that rainfall induced a change in deformation pattern both on the surface and the wall face. The rainfall induced more movement at the top part of the slope due to the weight of rain-water contained in the ASM bags before it flowed down to the sump. Thus, more movement was seen at the top part of the wall. This agrees with the field observation of earth pressure at depth of 1.5m from crest. The earth pressure cell indicated that rainfall infiltration affects the horizontal pressure in NS direction more than the vertical pressure in the top part of the wall.
5. Stability analysis of GBS slope shows that the local stability of the GBS was not affected by rainfall infiltration, therefore the load transferred to geogrids was constant. However, the global stability was influenced by the change in pore-water pressure distribution in the residual soil behind the GBS wall during rainfall.
6. Comparisons of the results of numerical analysis and field data indicate that the numerical procedure using deformation seepage analyses could be used to predict the pore-water pressure characteristics within the GBS slope.
7. The results from both field measurement and numerical analyses proved that the GBS slope performed well in minimizing rainwater infiltration and maintaining the stability of slope during rainfall.

Publications from MND-SUL Research Project

Journal Articles

1. Rahardjo, H, Q. Zhai, A. Satyanaga, E.C. Leong, C.L. Wang, and Johnny L.H Wong (2017) "Numerical Analyses for Assessment of Geobarrier System Performance", Geotechnical Special Publication (Accepted in October 2017).

2. Rahardjo, H., N. Gofar, F. Harnas and A. Satyanaga (2017) "Effect of Geobags on Water Flow through Capillary Barrier System", South East Asian Geotechnical Journal (Accepted in October 2017).

3. Rahardjo, H, A. Prasad, A. Satyanaga, H. Mohammad, E.C. Leong, C.L. Wang, and L.H Wong (2017) "1-D Infiltration Behavior of Two-layered Recycled Concrete Aggregates using Hydrophobic Materials in a Column Apparatus", ASCE Journal of Materials in Civil Engineering, March, DOI: 10.1061/(ASCE)MT.1943-5533.0001876 (Published online).

Journal Papers under Review

1. Rahardjo, H., Y. Kim, N. Gofar, E.C. Leong, C.L. Wang, and J.L.H. Wong. "Field instrumentations and monitoring of GeoBarrier System for steep slope protection", Transportation Geotechnics (under review – submitted November 2017).
2. Rahardjo, H, A. Satyanaga, Q. Zhai, E.C. Leong, J.H. Kew, C.L. Wang, and J.L.H Wong. "Performance of an instrumented slope protected by geobarrier system" Soils and Foundation (under review – submitted August 2017)
3. Rahardjo, H., N. Gofar, A. Satyanaga, E.C. Leong, C.L. Wang, and J.L.H. Wong. "Effect of rainfall infiltration on deformation of Geobarrier wall" Geotechnical and Geological Engineering Journal (under review – submitted September 2017)
4. Rahardjo, H, Q. Zhai, A. Satyanaga, E.C. Leong, W.K. Seow, W.K., C.L. Wang, and J.L.H. Wong. "Performance of capillary barrier as a sustainable slope protection" Canadian Geotechnical Journal (under review – submitted October 2017)

Conference Papers

1. Rahardjo, H, Q. Zhai, A. Satyanaga, E.C. Leong, C.L. Wang, and Johnny L.H Wong (2017) INVITED SPEAKER "Numerical Analyses for Assessment of Geobarrier System Performance", Proceedings of the 2nd Pan American Conference on Unsaturated Soils, 12-15 Nov 2017, Dallas, Texas, USA.
2. Rahardjo, H., C.L., Wang, A. Satyanaga. (2017) "Slope Protection against Rainfall-induced Slope Failure", INVITED SPEAKER, TC106 Workshop on The State of Practice in Unsaturated Soil Mechanics, 20 September 2017, Seoul, South Korea
3. Rahardjo, H., Q. Zhai., A. Satyanaga., E.C. Leong., C.L. Wang, and J.L.H. Wong (2016), "Field instrumentation for performance assessment of Geobarrier System", Proceedings of E-UNSAT 2016, 3rd European Conference on Unsaturated Soils, 12-14 September 2016, Paris, France.
4. Harnas, F.R., H. Rahardjo, A. Satyanaga and E.C Leong (2016), " Effectiveness of Dual Capillary Barrier as slope protection", Proceedings of the 12th International Symposium on Landslides, 12-19 June 2016, Napoli, Italy, pp. 1069-1075.
5. Rahardjo, H., Q. Zhai, A. Satyanaga, E.C. Leong, C. L. Wang and L.H. Wong (2015), "Geo-Barrier System as a retaining structure". Proceedings of AP-UNSAT2015 Conference, 23-26 Oct 2015, Guilin, China, pp. 871-876.

References

Agus, S. S., Leong, E. C., & Rahardjo, H. 2001. Soil-water Characteristic Curves of Singapore Residual Soils, Journal of Geotechnical and Geological Engineering, 19(4):285-309.

Ansari, Y., Merifield, R., Yamamoto, H., & Sheng, D. 2011. Numerical analysis of soilbags under compression and cyclic shear. Computers and Geotechnics 38: 659–688.

ASTM D7830 / D7830M-13. 2013. Standard Test Method for In-Place Density (Unit Weight) and Water Content of Soil Using an Electromagnetic Soil Density Gauge. ASTM International, West Conshohocken, PA.

ASTM D698-12. 2012. Standard Test Methods for Laboratory Compaction Characteristics of Soil Using Standard Effort (12 400 ft-lbf/ft^3 (600 kN-m/m^3)). ASTM International. West Conshohocken, PA.

ASTM D2487-11. 2011. Standard Practice for Classification of Soils for Engineering Purposes (Unified Soil Classification System). ASTM International. West Conshohocken, PA.

ASTM D7181-11. 2009. Method for Consolidated Drained Triaxial Compression Test for Soils. ASTM International, West Conshohocken, PA.

ASTM D4767-04. 2009. Test method for consolidated undrained triaxial compression test for cohesive soils. ASTM International. West Conshohocken, PA.

ASTM D7181-11. 2009. Method for Consolidated Drained Triaxial Compression Test for Soils. ASTM International, West Conshohocken, PA.

ASTM D6838-02. 2008. Standard Test Methods for Determination of the Soil Water Characteristic Curve for Desorption Using Hanging Column, Pressure Extractor, Chilled Mirror Hygrometer, or Centrifuge. ASTM International, West Conshohocken, PA.

ASTM D 4318–00. 2000. Standard Test Methods for Liquid Limit, Plastic Limit, and Plasticity Index of Soils. ASTM International, West Conshohocken, PA.

Fredlund, D. G., Rahardjo, H. & Fredlund, M. D. 2012. Unsaturated Soil Mechanics in Engineering Practice. John Wiley & Sons, Inc. 926p.

Fredlund, D. G. & Xing, A. 1994. Equations for the Soil-Water Characteristic Curve. Canadian Geotechnical Journal. 31:521-532.

Fredlund, D. G., & Rahardjo, H. 1993. Soil Mechanics for Unsaturated Soils. John Wiley & Sons, Inc., 517p.

Geoslope International Pte. Ltd. 2012a. SIGMA/W User's Guide for Slope Stability Analysis. Geoslope International Ltd., Calgary, Alberta, Canada.

Geoslope International Pte. Ltd. 2012b. SLOPE/W User's Guide for Slope Stability Analysis. Geoslope International Ltd., Calgary, Alberta, Canada.

Green, R. E. & Corey, J. C. 1971. Calculation of Hydraulic Soils, Prediction, Laboratory Test and In-Situ Measurements. Proc. 8th Intl. Conf. Soil Mechanics and Foundation Engineering, Moscow, Russia, pp. 163-170.

Harnas, F.R. Rahardjo, H. Satyanaga, A. & Leong, E.C. 2016a. Effectiveness of Dual Capillary Barrier as slope protection. Proc.12th International Symposium on Landslides, Napoli, Italy, pp.1069-1075.

Harnas, F.R. Rahardjo, H. Leong, E.C. & Wang, J.Y. 2016b. Physical Model for the Investigation of Capillary Barriers Performance Made Using Recycled Asphalt. Geotechnical Testing Journal, ASTM International, 39(6):977-990.

Harnas, F.R. Rahardjo, H. Leong, E.C. & Wang, J.Y. 2014a. An Experimental Study on Dual Capillary Barrier using Recycled Asphalt Pavement Materials. Canadian Geotechnical Journal, 51(10):1165-1177

Harnas, F.R. Rahardjo, H. Leong, E.C. & Wang, J.Y. 2014b. Effect of Evaporation on the Performance of Capillary Barriers with Recycled Asphalt Material. Proc. 14th Intl. Conf. Intl. Assoc. Computer Methods & Advances in Geomechanics. Kyoto, Japan.

Head, K. H. (1986) *Manual of Soil Laboratory Testing*. Vol. 2&3, Effective Stress Tests, 1st ed., ELE International Ltd.

Indrawan, I.G.B. & Rahardjo, H. 2010. Water Infiltration through Capillary Barrier Models. Proc. Symp. Protecting Life from Geo-Disaster and Environmental Hazards. Bali, Indonesia. pp. 439-446

Koerner, R.M. & Koerner, G.R. 2013. A data base, statistics and recommendations regarding 171 failed geosynthetic reinforced mechanically stabilized earth (MSE) walls. Geotextiles and Geomembranes 40 (2013) 20-27

Koerner, R.M. 20012. Designing with Geosynthetics, 6th ed. Prentice Hall. 796 p.

Krisdani, H. Rahardjo, H. & Leong, E.C. 2010. Application of Geosynthetic Material as a Coarse-grained Layer in Capillary Barriers. Special Issue on Unsaturated Geosynthetics. Geosynthetics International Journal 17(5):323–331.

Krisdani, H. Rahardjo, H. & Leong, E.C. 2006. Experimental Study of 1-D Capillary Barrier Model using Geosynthetic Material as the Coarse-Grained Layer. Proc. 4th Intl. Conf. Unsaturated Soils. Geo Institute. Phoenix, USA.:1683– 1694.

Krisdani, H. Rahardjo, H. & Leong, E.C. 2005. Behaviour of Capillary Barrier System Constructed using Residual Soil. Proc. Geo-Frontiers Conf. on Innovative Barriers and Barrier Materials, Austin, USA.: 1–15.

Kunze, R. J., Uehara, G., & Graham, K. (1968) Factors Important in the Calculation of Hydraulic Conductivity. *Proceeding of Soil Science Society,* America, 32 760-765.

Leong, E.C., & Wijaya, M. 2015. Universal soil shrinkage curve equation. Geoderma, January, 237–238:78-87.

Leong, E. C., & Rahardjo, H. (1997) Permeability Functions for Unsaturated Soils. *Journal of Geotechnical and Geoenvironmental Engineering, ASCE,* 123(12), 1118-1126.

Liu, C.N., Yang, K.Y., Ho, Y.H. & Chang, C.M. 2012. Lessons learned from three failures on a high steep geogrid-reinforced slope. Geotextiles and Geomembranes 34: 131 – 143.

Marshall, T. J. (1958) A Relation Between Permeability and Size Distribution of Pores. *Journal Soil Science,* 9, 1-8.

Matsuoka, H., & Liu, S. 2006. A new earth reinforcement method using soilbags. London. Taylor and Francis

McCulloch, T., Kang, D., Shamet, R., Lee, S.J. & Nam, B.H. 2017. Long-Term Performance of Recycled Concrete Aggregate for Subsurface Drainage. Journal of Performance of Constructed Facilities, 31(4).

Millington, R. J., & Quirk, J. P. (1961) Permeability of Porous Solids. *Trans. Faraday Soc.*, 57, 1200-1207.

Millington, R. J., & Quirk, J. P. (1959) Permeability of Porous Media. Nature, Land, 183, 387-388.

NParks Board Singapore 2013. Specifications of Soil Mixture for General Landscapping Use. CEGE Publication No CS. AO3. 2013. 20pp.

Rahardjo, H. Nong, X.F. Lee, D.T.T., Leong, E.C. & Fong, Y.K. 2018a. Expedited soil–water characteristic curve tests using combined centrifuge and chilled mirror techniques. Geotechnical Testing Journal. ASTM International. January.

Rahardjo, H., Gofar, N., Harnas, F. & Satyanaga, A. 2018b. Effect of Geobags on Water Flow through Capillary Barrier System. Geotechnical Engineering Journal of the SEAGS & AGSSEA 49(2)

Rahardjo, H, Zhai, Q. Satyanaga, A. Leong, E.C. Wang, C.L & Wong, JLH. 2017a. Invited Speaker. Numerical Analyses for Assessment of Geobarrier System Performance. Proc. 2nd Pan American Conf. Unsaturated Soils, Dallas, Texas, USA.

Rahardjo, H., Wang, C.L. Satyanaga, A. 2017b. Slope Protection against Rainfall-induced Slope Failure. Invited Speaker. TC106 Workshop on The State of Practice in Unsaturated Soil Mechanics. Seoul, South Korea.

Rahardjo, H., Krisnanto, S. & Leong, E.C. 2016a. Effectiveness of Capillary Barrier and Vegetative Slope Covers in Maintaining Soil Suction, Soils and Rocks Journal, Special topic on Theory and Practice of Unsaturated Soils Mechanics. 39(1):51-69

Rahardjo, H., Satyanaga, A., Harnas, F.R. & Leong, E.C. 2016b. Use of Dual Capillary Barrier as Cover System for a Sanitary Landfill in Singapore, Indian Geotechnical Journal. 46(3):228-238.

Rahardjo, H. 2015. Capillary Barrier as a Slope Protection. Distinguished Lecture, Proc. AP-UNSAT2015. Guilin, China. pp. 23-36.

Rahardjo, H. Zhai, Q., Satyanaga, A., Leong, E.C., Wang, C.L. & Wong, J.L.H. 2015. Geo-Barrier System as a retaining structure. Proc. AP-UNSAT2015. Guilin, China. pp. 871-876.

Rahardjo, H., A. Satyanaga, E.C. Leong & J.Y. Wang. 2013a. Unsaturated Properties of Recycled Materials. Engineering Geology. 161: 44-54.

Rahardjo, H., Santoso, V. A., Leong, E. C., Ng, Y. S., Tam C.P.H. & Satyanaga A. 2013b. Use of recycled crushed concrete and Secudrain in capillary barriers for slope stabilization. Canadian Geotechnical Journal 50: 1-12.

Rahardjo, H., Satyanaga, A., Harnas, F.R. Wang, J.Y. & Leong, E.C. 2013c. Capillary Barrier System for Landfill Capping. Proc. Coupled Phenomena in Environmental Geotechnics (CPEG), a TC 215 Symposium. Torino, Italy

Rahardjo, H., Santoso, V. A., Leong, E. C., Ng, Y. S. & Hua, C. J. 2012a. Performance of an Instrumented Slope Covered by a Capillary Barrier System. ASCE Journal of Geotechnical and Geoenvironmental Engineering. 138(4):481-490.

Rahardjo, H., Santoso, V. A., Leong, E. C., Ng, Y. S. & Hua, C. J. 2012b. Use of Recycled Concrete Aggregates in a Capillary Barrier for Slope Stability. Proc. 11th Intl. & 2nd North American Symposium on Landslides – ISL NASL 2012, Banff, Canada.

Rahardjo, H., Hua, C.J. Leong, E.C. & V.A. Santoso 2010. Performance of an Instrumented Slope under a Capillary Barrier System. Proc. of 5th Intl. Conf. Unsaturated Soils, Barcelona, Spain, Vol. 2, pp. 1279-1284.

Rahardjo, H., Krisdani, H. & Leong, E.C. 2007a. Application of Unsaturated Soil Mechanics in Capillary Barrier System. Invited lecture. Proc. 3rd Asian Conference on Unsaturated Soils. Nanjing, China. pp. 127–137.

Rahardjo, H., Satyanaga, A. & Leong, E.C. 2007b. Unsaturated Soil Mechanics for Slope Stability. Invited Lecture. Proc. National Conference of Korean Geotechnical Society (KGS), Busan, Korea. pp. 1-21.

Rahardjo, H., Tami, D. & Leong, E.C. 2006. Effectiveness of Sloping Capillary Barriers under High Precipitation Rates. Keynote Lecture. Proc. 2nd Intl. Conf. Problematic Soils, Petaling Jaya, Malaysia. pp. 39 – 54.

Schiendler, U., Duiner, W., Unold, G.V., Mueller, L. & Wieland, R. 2010. The evaporation method: Extending the measurement range of soil hydraulic properties using the air entry pressure of ceramic cup, Journal of Plant Nutritional and Soil Science 173:563-572.

Smesrud, J. & Selker, J. 2001. Effect of Soil-Particle Size Contrast on Capillary Barrier Performance. ASCE Journal of Geotechnical and Geoenvironmental Engineering. 127(10): 885-888.

Tami, D. Rahardjo, H. Leong, E.C. & Fredlund, D.G. 2004a. Design and Laboratory Verification of a Physical Model of Sloping Capillary Barrier. Canadian Geotechnical Journal. 41(5):814–830.

Tami, D. Rahardjo, H. Leong, E.C. & Fredlund, D.G. 2004b. A Physical Model for Sloping Capillary Barriers. Geotechnical Testing Journal. ASTM International. 27(2):173-183.

Tami, D. Rahardjo, H. & Leong, E.C. 2003. Comparison of numerical and experimental data from a capillary barrier model. Proc. 2nd Asian Conference on Unsaturated Soils. Geotechnical and Geoenvironmental Issues. Osaka, Japan, pp. 351-356.

Tami, D. Rahardjo, H. & Leong, E.C. 2002. Laboratory Model of Capillary Barrier. Proc. Intl. Workshop Environmental Geomechanics, Ascona, Switzerland, pp. 267-273.

Xiaoli Fu, Shao, M., Lu, D. & Wang, H. 2011. Soil water characteristic curve measurement without bulk density changes and its implications in the estimation of soil hydraulic properties. Geoderma, 167–168:1-8.

Yang, H. Rahardjo, H. Leong, E.C. & Fredlund, D.G. 2004. A Study of Infiltration on Three Sand Capillary Barriers. Canadian Geotechnical Journal, 41(4):629–643.

Yoo, C. & Jung, H.Y. 2006. Case History of Geosynthetics Reinforced Segmental Retaining Wall Failure. ASCE Journal of Geotechnical and Geoenvironmental Engineering, 132(12): 1538-1548.

Zhai, Q., & Rahardjo, H., (2012) Determination of soil-water characteristic curve variables. *Computer and Geotechnics*, 42, pp. 37-43.

Note: The publications written in bold font are NTU publications related to Capillary Barrier and Geobarrier (GBS) systems